Published for SISSA by Springer

Received: October 17, 2016
Accepted: November 16, 2016
Published: December 5, 2016

Factorization for the light-jet mass and hemisphere soft function

Thomas Becher,[a] **Benjamin D. Pecjak**[b] **and Ding Yu Shao**[a]

[a] *Albert Einstein Center for Fundamental Physics, Institut für Theoretische Physik, Universität Bern, Sidlerstrasse 5, CH-3012 Bern, Switzerland*

[b] *Institute for Particle Physics Phenomenology, University of Durham, DH1 3LE Durham, United Kingdom*

E-mail: becher@itp.unibe.ch, ben.pecjak@durham.ac.uk, shao@itp.unibe.ch

Abstract: Many collider observables suffer from non-global logarithms not captured by standard resummation techniques. Classic examples are the light-jet mass event shape in the limit of small mass and the related hemisphere soft function. We derive factorization formulas for both of these and explicitly demonstrate that they capture all logarithms present at NNLO. These formulas achieve full scale separation and provide the basis for all-order resummations. A characteristic feature of non-global observables is that the soft radiation is driven by multi-Wilson-line operators, and the ones arising here map onto those relevant for the case of narrow-cone jet cross sections. Numerically, the contributions of non-global logarithms to resummed hemisphere-mass event shapes are sizeable.

Keywords: Effective field theories, Perturbative QCD, Renormalization Group, Resummation

ArXiv ePrint: 1610.01608

doi:10.1007/JHEP12(2016)018

JHEP12(2016)018

Contents

JHEP12(2016)018

1 Non-global logarithms in hemisphere-mass observables

Perturbative corrections to observables which involve a hierarchy of scales are enhanced by logarithms of the scale ratios. Starting with the pioneering work of Sudakov [1], methods were developed to resum such logarithmically enhanced corrections to all orders. A crucial simplification is exponentiation, the statement that the leading logarithms can be obtained from exponentiating the leading-order correction to a process. Effective field theories provide a modern way to analyze multi-scale problems. In these theories exponentiation is a consequence of the renormalization group (RG). The logarithms are resummed by evolving Wilson coefficients, which encode the physics associated with high scales, down to lower scales and the leading-order solution of the RG equation is an exponential.

Interestingly, this simple exponentiation property does not hold for all observables. For example, if one considers interjet energy flow, one finds that the relevant wide-angle soft radiation produces a very intricate pattern of leading logarithms [2]. Instead of a simple linear evolution equation, one needs to solve a complicated non-linear integral equation to obtain the leading logarithms, the Banfi-Marchesini-Smye (BMS) equation [3]. Interjet

energy flow is an example of a non-global observable. Such observables are insensitive to radiation in certain regions of phase space (the inside of the jets, for the case of the interjet energy flow) and the same complicated pattern of "non-global" logarithms is present in all of them. Perhaps the simplest quantity which suffers from such logarithms is the hemisphere soft function, which is obtained by considering the radiation from two Wilson lines in opposite directions. Allowing for large energy in one hemisphere, but only a small amount in the other leads to non-global logarithms. This soft function is also relevant in the context of the light-jet mass event shape in e^+e^- collisions, in which the complicated pattern of logarithms was originally discovered [4].

The BMS equation makes crucial use of the simple form of strongly ordered gluon-emission amplitudes. Beyond leading logarithmic accuracy these simplifications do not apply and it was therefore not clear how to generalize the BMS equation to higher accuracy. In the past few years, the problem of non-global logarithms has received renewed interest, in particular in the context of Soft-Collinear Effective Theory (SCET) [5–7] (see [8] for a review). Several papers have computed hemisphere soft functions up to next-to-next-to-leading order (NNLO) to obtain full results for their non-global structure at this order [9–12]. Furthermore, by perturbatively expanding the BMS equation, the analytic form of the leading-logarithmic terms up to five-loop order was extracted [13, 14]. Using an efficient new method to perform the angular integrations [15], this result has now been extended to 12 (!) loops [16].[1] In addition to these fixed-order considerations, a method to approximately resum the non-global logarithms was proposed [17, 18]. At leading-logarithmic accuracy it reduces to an iterative solution of the BMS equation [19].

In the recent papers [20, 21], two of us have analyzed cone-jet cross sections and have derived factorization theorems for the case where the outside energy is small. The characteristic feature of these theorems is the presence of multi-Wilson-line operators which describe the soft emissions from energetic partons inside jets. In our effective-field-theory framework, the non-global logarithms are obtained from an RG-evolution equation which generalizes the BMS equation to arbitrary logarithmic accuracy. The complicated structure arises because operators with an arbitrary number of soft Wilson lines are present in the factorization theorem. To obtain the large logarithms, one needs to exponentiate an infinite-dimensional anomalous-dimension matrix, which, at leading-logarithmic accuracy and large N_c, is equivalent to solving the BMS equation. The exponentiation property mentioned earlier is thus present also for non-global logarithms, but takes a very complicated form. Our framework is closely related to the one proposed in [22] and involves the same anomalous dimension, which was computed to two-loop order in that reference and has recently even been derived at three-loop accuracy in the planar limit in $\mathcal{N} = 4$ super Yang-Mills theory [15].

To make contact with the previous literature which has focused mostly on the hemisphere soft function, it is important to analyze this quantity using our framework. We do this in the present paper and at the same time also derive a factorization theorem for the light-jet mass event shape. To define this e^+e^- event shape, one first introduces the

[1] Plots of the result are shown in [19].

JHEP12(2016)018

thrust axis $\vec{n}$ as the direction of maximum momentum flow. More precisely, the unit vector $\vec{n}$ is chosen to maximize the quantity $\sum_i |\vec{n}\cdot\vec{p}_i|$, where the sum runs over all particles in the final state. The event shape thrust is defined as this sum normalized to Q, where Q is the center-of-mass energy of the collision. The thrust axis splits each event into two hemispheres, which can arbitrarily be labelled as "left" and "right", and one can define additional event shapes by considering the invariant masses M_L and M_R of the particles in the hemispheres. Two commonly used event shapes are

$$\text{heavy-jet mass:} \quad \rho_h = \frac{1}{Q^2}\max(M_L^2, M_R^2)\,, \tag{1.1}$$

$$\text{light-jet mass:} \quad \rho_\ell = \frac{1}{Q^2}\min(M_L^2, M_R^2)\,. \tag{1.2}$$

In the limit where the jet masses become small, perturbative corrections to these observables are logarithmically enhanced. For the heavy-jet mass these logarithms have been resummed up to next-to-next-to-next-to-leading logarithmic (N^{3}LL) accuracy [23], while only NLL predictions are available for the light-jet mass ρ_ℓ [4, 24]. The reason for the poor accuracy for ρ_ℓ was that it was not known how this non-global observable factorizes in the limit of small ρ_ℓ, while the factorization is well known for the heavy-jet mass.

Due to left-right symmetry, the three possible scale hierarchies for the hemisphere masses are a.) $M_L \sim M_R \ll Q$, b.) $M_L \ll M_R \ll Q$ and c.) $M_L \ll M_R \sim Q$. The relevant factorization theorem for case a.) has the form [25]

$$\frac{d\sigma}{dM_L^2 dM_R^2} = \sigma_0 H(Q^2)\int_0^\infty d\omega_L \int_0^\infty d\omega_R J_q(M_L^2 - Q\omega_L) J_q(M_R^2 - Q\omega_R) S(\omega_L,\omega_R)\,, \tag{1.3}$$

where σ_0 is the Born level cross section. The hard function H collects the virtual corrections to $\gamma^* \to q\bar{q}$ which are known to three loops [26, 27]. The jet function J_q is the usual inclusive jet function in SCET, which is known to two loops [28, 29]. The hemisphere soft function $S(\omega_L,\omega_R)$ is a matrix element of Wilson lines along the two jet directions and is also known at NNLO [9, 10, 30]. This function measures the contribution of the soft radiation to the hemisphere mass in each hemisphere. Since the relevant anomalous dimensions are known for all ingredients in (1.3), one can solve their RG evolution equations to obtain N^{3}LL resummation for hierarchy a.) which is the one relevant for the heavy-jet mass ρ_h.

However, the above theorem does not achieve resummation for case b.) since for $\omega_L \ll \omega_R$ the soft function $S(\omega_L,\omega_R)$ itself contains large logarithms of $\kappa = \omega_L/\omega_R$, which are examples of non-global logarithms. To be able to resum also these logarithms one must factorize the physics at the two different soft scales ω_L and ω_R. In the context of the function $S(\omega_L,\omega_R)$, we will refer to ω_R as the hard scale and ω_L the soft one. One of the main results of the present paper is that the hemisphere soft function factorizes in the limit $\kappa \to 0$ as

$$S(\omega_L,\omega_R) = \sum_{m=0}^{\infty} \big\langle \boldsymbol{\mathcal{H}}_m^S(\{\underline{n}\},\omega_R) \otimes \boldsymbol{\mathcal{S}}_{m+1}(\{n,\underline{n}\},\omega_L)\big\rangle\,. \tag{1.4}$$

The hard functions $\boldsymbol{\mathcal{H}}_m^S$ are the squared amplitudes for m-parton emissions from the two Wilson lines in the hemisphere soft function into the right hemisphere, integrated over their

JHEP12(2016)018

energies but at fixed directions $\{\underline{n}\} = \{n_1, \ldots, n_m\}$, where the n_i's are light-like vectors. The soft functions $\boldsymbol{\mathcal{S}}_{m+1}$ consist of $m+2$ Wilson lines along the directions $\{\underline{n}\}$ of the m hard partons and the two jets along $n^\mu = (1, \vec{n})$ and $\bar{n}^\mu = (1, -\vec{n})$. Both of these are matrices in color space [32, 33], and $\langle \ldots \rangle$ indicates a sum over color indices. The symbol $\otimes$ indicates that one has to integrate over the m directions of the emissions into the right hemisphere. The form of the factorization theorem (1.4) is basically the same as the one for wide-angle cone-jet cross sections derived in [20]. To see the connection, one should view the right hemisphere as the inside of a jet which contains hard particles with momenta $p^\mu \sim \omega_R$ and the left hemisphere as the outside region where a veto on radiation is imposed which constrains the momenta to $p^\mu \sim \omega_L$.

Before analyzing the factorization formula (1.4) in more detail and providing operator definitions for its ingredients, we now turn to the light-jet mass ρ_ℓ. Due to left-right symmetry and its definition, ρ_ℓ is directly related to the left-jet mass $\rho_L = M_L^2/Q^2$ according to

$$\frac{d\sigma}{d\rho_\ell} = 2\frac{d\sigma}{d\rho_L} - \frac{d\sigma}{d\rho_h}\bigg|_{\rho_L=\rho_h=\rho_\ell} . \tag{1.5}$$

Instead of the light-jet mass one can therefore equally well analyze the factorization for ρ_L. If one only measures the left-jet mass, the mass of the right jet will typically be large, so that scale hierarchy c.) applies. We find that the cross section for the left-jet mass factorizes as

$$\frac{d\sigma}{dM_L^2} = \sum_{i=q,\bar{q},g} \int_0^\infty d\omega_L \, J_i(M_L^2 - Q\,\omega_L) \sum_{m=1}^\infty \left\langle \boldsymbol{\mathcal{H}}_m^i(\{\underline{n}\}, Q) \otimes \boldsymbol{\mathcal{S}}_m(\{\underline{n}\}, \omega_L) \right\rangle . \tag{1.6}$$

Since the unobserved radiation in the right hemisphere is typically hard, such that $p^\mu \sim Q$, we no longer encounter a jet function for this hemisphere, in contrast to the previous case (1.3). The hard functions also differ from the function $\boldsymbol{\mathcal{H}}_m^S$ encountered for the hemisphere soft functions. Rather than Wilson-line matrix elements as in (1.4), the functions $\boldsymbol{\mathcal{H}}_m^i$ in this case are given by squared QCD amplitudes with a single parton of flavor i in the left hemisphere propagating along the $\bar{n}$-direction and m partons in the right hemisphere. The subsequent branchings of the hard parton on the left are described by the jet functions J_i. A graphical representation of the factorization theorems is shown in figure 1.

Our paper is organized as follows. In the next section, we will flesh out the factorization formulas for the hemisphere soft function and for the light-jet mass event shape and discuss their derivation, which can be obtained following similar steps as in [20]. The soft functions in these theorems can be related to the coft functions computed in that reference so that the only new ingredients to our factorization formulas are the hard functions. After computing these in section 3 up to $\mathcal{O}(\alpha_s^2)$, we verify that we reproduce the known NNLO result for the hemisphere soft function in the limit $\omega_L \to 0$. Next, we analyze the light-jet mass distribution in section 4 and compare to the numerical fixed-order result for this quantity. In section 5 we use the known result for the leading non-global logarithms in the hemisphere soft function to obtain numerical results for the light-jet mass at NLL accuracy. In section 6 we discuss the necessary steps to perform higher-order resummation for this event shape and conclude.

JHEP12(2016)018

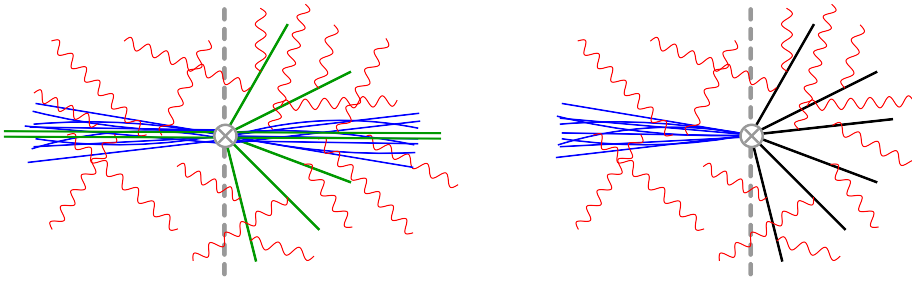

Figure 1. Pictorial representation of the factorization theorems for the differential cross sections with respect to the hemisphere jet masses in the limit $M_L \ll M_R \ll Q$ (left), and to the left-jet mass when $M_L \ll M_R \sim Q$ (right). Blue lines correspond to collinear partons inside the jet functions, the red lines represent soft emissions. The green lines in the left picture correspond to the hard part of the hemisphere soft function, while the black lines in the right picture correspond to hard emission into the right hemisphere.

2 Factorization

The derivation of the factorization formula follows the same steps in both cases and is similar to the one relevant for wide-angle cone-jet cross sections presented in [20]. We will first sketch the derivations of the theorems and specify the ingredients. We then relate the soft functions to the ones which arise in the case of the narrow-cone jet cross sections. Due to this relation, we can use the results [20] for these and only the hard functions need to be computed.

2.1 Hemisphere soft function

The hemisphere soft function describes radiation originating from a quark and an anti-quark along the directions n and $\bar{n}$ of the two jets. Their soft radiation is described by Wilson lines. The one generated by the outgoing quark along the n direction is

$$S(n) = \boldsymbol{P} \exp\left(ig_s \int_0^\infty ds\, n\cdot A^a(sn) t^a\right), \tag{2.1}$$

and the soft function is defined as

$$S(\omega_L,\omega_R) = \frac{1}{N_c}\sum_X \mathrm{Tr}\langle 0|S(\bar{n})S^\dagger(n)|X\rangle\langle X|S(n)S^\dagger(\bar{n})|0\rangle \delta(\omega_R - n\cdot P_R)\,\delta(\omega_L - \bar{n}\cdot P_L)\,, \tag{2.2}$$

where the trace is over color indices. We call the hemisphere which contains the thrust vector the right hemisphere. The right-moving particles therefore have $\bar{n}\cdot p > n\cdot p$ and $P_{R(L)}$ is the total momentum in the right (left) hemisphere. Usually, the function $S(\omega_L,\omega_R)$ is defined in terms of the soft gluon field in SCET. However, the soft SCET Lagrangian is equivalent to the full QCD one so for our discussion we will consider (2.2) as a matrix element in QCD. In the asymmetric case $\omega_L \ll \omega_R$ the function $S(\omega_L,\omega_R)$ develops large, non-global logarithms (NGLs) in the ratio $\kappa \equiv \omega_L/\omega_R \ll 1$. It is these logarithms which we seek to resum using effective-field-theory methods.

JHEP12(2016)018

Before constructing the appropriate effective theory, it is useful to study the structure of NGLs in the matrix element (2.2) perturbatively. Clearly, one method is to calculate the hemisphere soft function at a given order in perturbation theory, and then take the limit $\kappa \to 0$ in the final result. This was the approach taken in the NNLO calculations of [9, 10], and the obvious benefit of such a computation is that it provides the hemisphere soft function for any value of κ. On the other hand, if one is interested only in NGLs appearing in the limit $\kappa \to 0$, it is much simpler to obtain results by expanding the phase-space integrals appearing in the hemisphere soft function using the method of regions [31]. Indeed, in a first step we have used this method to reproduce the NNLO fixed-order calculations in the non-global limit. The factorization results discussed below can be viewed as a translation of this diagrammatic approach into the language of effective field theory.

We find that two momentum regions are needed for the leading-power diagrammatic expansion in the limit $\kappa \to 0$. Defining the light-cone components of an arbitrary vector p as $(n \cdot p, \bar{n} \cdot p, p_\perp)$, these regions are specified by the scalings

$$\begin{aligned} \text{hard:} \quad & p_h \sim \omega_R \,(1,1,1)\,, \\ \text{soft:} \quad & p_s \sim \omega_R \,(\kappa,\kappa,\kappa)\,. \end{aligned} \tag{2.3}$$

The homogeneous scaling of the momentum components arises because the soft and hard radiation covers a wide angular range so that no specific direction is singled out. The expansion of individual diagrams also receives contributions from a left-collinear mode scaling as $\omega_R(1, \kappa, \sqrt{\kappa})$. However, in the sum of all diagrams these collinear contributions vanish, and in appendix A we present an all-orders proof of this result, based on the invariance of Wilson lines under rescalings of the reference vector.

A non-trivial interplay between contributions of the two regions is responsible for the structure of NGLs in the hemisphere soft function. By NGLs, we mean contributions which cannot be written as a naive product of two component functions depending on ω_L and ω_R only.[2] An NLO analysis does not reveal the presence of NGLs, since the NLO result is the sum of the identical contributions of a single hard emission into the right hemisphere and a single soft emission into the left hemisphere, which can always be written as the product of identical one-scale functions for the hard and soft regions. At NNLO, on the other hand, it is possible for a virtual gluon to split into two particles flying into different hemispheres, and it is obvious that a simple product structure is insufficient to describe these contributions since they have a different color structure. Two types of opposite-hemisphere configurations are relevant. The first involves a soft gluon in the left hemisphere and a hard gluon in the right hemisphere and gives rise to double and single NGLs. The second involves one soft gluon in each hemisphere. Such a configuration is not possible for hard radiation, because a hard emission into the left hemisphere would violate the scaling $\omega_L \ll \omega_R$. This asymmetry between double-hard and double-soft contributions generates the remaining single NGLs needed to reproduce the known NNLO result in the $\kappa \to 0$ limit.

[2]The exact definition of NGLs is ambiguous; we consider several possibilities below in the discussion following (3.35).

JHEP12(2016)018

The effective field theory appropriate for describing the situation above has recently been developed in [20, 21]. The basic observation of these papers was that each of the hard partons generates a soft Wilson line along its direction, so even though hard and soft contributions factorize in (1.4), new hard and soft functions appear at each order in perturbation theory. To obtain the operators in the low-energy effective theory, one therefore first considers a kinematic configuration with m hard partons along fixed directions and then introduces a soft Wilson line for each of them. The amplitudes for the emissions of m hard partons with momenta $\{\underline{p}\} = \{p_1, \cdots, p_m\}$ from the two Wilson lines in (2.2) take the form

$$|\mathcal{M}_m^S(\{\underline{p}\})\rangle = \langle\{\underline{p}\}|S(n)S^\dagger(\bar{n})|0\rangle\,. \tag{2.4}$$

Note that on the left-hand side of the above equation we use the color-space formalism of [32, 33] in which the amplitude $|\mathcal{M}_m^S(\{\underline{p}\})\rangle$ is a vector in the color space of the m partons. However, on the right-hand side the color indices of the m partons are suppressed and the bra-ket notation denotes states in the Hilbert space. The superscript S indicates that the amplitude $\mathcal{M}_m^S$ is obtained from the Wilson line matrix element.

A general soft Wilson line along the light-like direction $n_i \propto p_i$ is defined in analogy with (2.1) as

$$\boldsymbol{S}_i(n_i) = \mathbf{P}\exp\left(ig_s\int_0^\infty ds\, n_i\cdot A_s^a(sn_i)\,\boldsymbol{T}_i^a\right), \tag{2.5}$$

where the color matrices for the representation of the underlying particle i are denoted by $\boldsymbol{T}_i^a$. On the amplitude level, the soft radiation from the two original Wilson lines and the additional hard partons is obtained from the Wilson-line operator

$$\boldsymbol{S}_a(\bar{n})\,\boldsymbol{S}_b(n)\,\boldsymbol{S}_1(n_1)\ldots\boldsymbol{S}_m(n_m)|\mathcal{M}_m^S(\{\underline{p}\})\rangle\,, \tag{2.6}$$

where $\boldsymbol{S}_a(\bar{n})$ and $\boldsymbol{S}_b(n)$ are the anti-quark and quark Wilson lines present in the original definition (2.2). A derivation of the formula (2.6) from SCET was given in [20].

To obtain the factorized result for the cross section we need to square the factorized amplitude (2.6), integrate over the energies and directions of the hard partons, and add up the contributions from different multiplicities of hard partons. Doing so, we obtain the factorization formula (1.4) for the hemisphere soft function in the limit $\kappa \to 0$. The definitions of the hard functions in this formula read

$$\boldsymbol{\mathcal{H}}_m^S(\{\underline{n}\},\omega_R) = \prod_{i=1}^m \int \frac{dE_i\,E_i^{d-3}}{(2\pi)^{d-2}}\,|\mathcal{M}_m^S(\{\underline{p}\})\rangle\langle\mathcal{M}_m^S(\{\underline{p}\})|\,\delta(\omega_R - n\cdot P_R)\,\Theta_R\big(\{\underline{p}\}\big)\,, \tag{2.7}$$

where d is the number of spacetime dimensions. The theta function Θ_R ensures that all hard partons are inside the right hemisphere so that P_R is simply the total hard momentum. Note that the directions of the hard partons are fixed. The integral over the directions is performed after multiplication with the soft function, which for m additional hard partons is obtained from squaring the Wilson-line operator matrix elements

$$\begin{aligned}\boldsymbol{\mathcal{S}}_{m+1}(\{n,\underline{n}\},\omega_L) =& \sum_{X_s}\langle 0|\,\boldsymbol{S}_a^\dagger(\bar{n})\,\boldsymbol{S}_b^\dagger(n)\,\boldsymbol{S}_1^\dagger(n_1)\ldots\boldsymbol{S}_m^\dagger(n_m)\,|X_s\rangle \\ &\times\langle X_s|\,\boldsymbol{S}_a(\bar{n})\,\boldsymbol{S}_b(n)\,\boldsymbol{S}_1(n_1)\ldots\boldsymbol{S}_m(n_m)\,|0\rangle\,\delta(\omega_L - \bar{n}\cdot P_L)\,.\end{aligned} \tag{2.8}$$

Note that the soft partons can be in either hemisphere. The ones in the left hemisphere contribute to ω_L, but the ones in the right hemisphere are not constrained because their contribution to ω_R is negligible compared to the hard partons. The strict expansion of the phase-space measure is crucial to achieve the desired factorization of scales and to avoid double counting of the contributions from different momentum regions.

2.2 Left-jet mass

The factorization for the left-jet mass distribution is rather similar to that for the hemisphere soft function, but the expansion parameter is $\lambda = \omega_L/Q$ and the relevant momentum scalings are

$$\begin{aligned} \text{hard:} \quad & p_h \sim Q\,(1,1,1)\,, \\ \text{soft:} \quad & p_s \sim Q\,(\lambda,\lambda,\lambda)\,, \\ \text{collinear:} \quad & p_c \sim Q\,(1,\lambda,\sqrt{\lambda})\,. \end{aligned} \tag{2.9}$$

To derive the factorization theorem (1.6) and obtain the hard functions $\boldsymbol{\mathcal{H}}_m^i(\{\underline{n}\},Q)$, one can first match onto a version of SCET with a collinear field along the $\bar{n}$-direction as well as m additional collinear fields along directions in the right hemisphere. Then one performs the usual decoupling transformation on the collinear fields [6], which gives rise to the relevant soft multi-Wilson-line operator. Finally one takes the matrix element where there is a single hard parton along each of the m directions in the right hemisphere, and a jet of partons along the $\bar{n}$-direction on the left. This yields the hard functions $\boldsymbol{\mathcal{H}}_m^i(\{\underline{n}\},Q)$ together with the jet function J_i. We refrain from going over this derivation in more detail since it involves, up to obvious modifications, exactly the same steps as the ones detailed for the wide-angle jet cross section in [20].

The explicit definition of the hard functions for the the decay of a virtual photon into a final state with m particles in the right hemisphere is

$$\begin{aligned} \boldsymbol{\mathcal{H}}_m^i(\{\underline{n}\},Q) = \frac{1}{2Q}\prod_{j=1}^{m}\int \frac{dE_j\,E_j^{d-3}}{(2\pi)^{d-2}}\,|\mathcal{M}_{m+1}^i(\{p_0,\underline{p}\})\rangle\langle\mathcal{M}_{m+1}^i(\{p_0,\underline{p}\})| \\ \times\,\Theta_R\big(\{\underline{p}\}\big)\,(2\pi)^d\,\delta(Q-E_{\text{tot}})\,\delta^{(d-1)}(\vec{p}_{\text{tot}})\,, \end{aligned} \tag{2.10}$$

where $p_0^\mu = Q\,\bar{n}^\mu/2$ is the momentum of the single hard parton of flavor $i \in \{q,\bar{q},g\}$ in the left hemisphere, and the amplitudes $|\mathcal{M}_{m+1}^i(\{p_0,\underline{p}\})\rangle$ are standard QCD amplitudes for the decay of the virtual photon into $(m+1)$ partons. The associated soft function is

$$\begin{aligned} \boldsymbol{\mathcal{S}}_m(\{\underline{n}\},\omega_L) = \sum\!\!\!\!\!\!\int_{X_s} \langle 0|\,\boldsymbol{S}_0^\dagger(\bar{n})\,\boldsymbol{S}_1^\dagger(n_1)\ldots\boldsymbol{S}_m^\dagger(n_m)\,|X_s\rangle \\ \times\,\langle X_s|\,\boldsymbol{S}_0(\bar{n})\,\boldsymbol{S}_1(n_1)\ldots\boldsymbol{S}_m(n_m)\,|0\rangle\,\delta(\omega_L-\bar{n}\cdot P_L)\,. \end{aligned} \tag{2.11}$$

This is exactly the same matrix element as (2.8) up to the fact that only the direction of the first Wilson line is fixed, as opposed to the case of the hemisphere soft function, where the first two, along the $\bar{n}$ and n directions, are kept fixed. We can thus get the one in (2.8) by taking the result for (2.11) and setting the reference vector of the second Wilson line to the n direction.

JHEP12(2016)018

Furthermore, almost the same matrix element as (2.11) has arisen in the context of narrow-cone jet cross sections. In that case, the Wilson line structure is associated with coft emissions which are simultaneously collinear and soft. Rather than a hemisphere constraint, the coft functions involve a constraint on out-of-jet radiation of the form $Q\beta > \bar{n}\cdot p_{\text{out}}$ and a particle is outside the right jet if $n\cdot p > \delta^2\,\bar{n}\cdot p$. If we set $\delta = 1$ and replace $Q\beta \to \omega_L$, the coft functions are mapped onto the left hemisphere (up to the fact that we impose the constraint as a δ-function instead of an upper limit). Since Wilson lines are invariant under a rescaling of the reference vector, the transformation maps the coft Wilson line matrix elements directly onto the soft functions (2.11) and we can use the results of [20, 21].

3 Hemisphere soft function at NNLO

In this section we demonstrate how our factorization formula can be used to reproduce the results for the hemisphere soft function at NNLO in perturbation theory in the asymmetric limit $\omega_L \ll \omega_R$. In the following, it will be convenient to work in Laplace space, where the convolutions in the factorization formulas (1.3) and (1.6) turn into products. We define the renormalized, Laplace-transformed soft function as

$$\tilde{s}(\tau_L,\tau_R,\mu) = \int_0^\infty d\omega_L \int_0^\infty d\omega_R\, e^{-\omega_L/(\tau_L e^{\gamma_E})} e^{-\omega_R/(\tau_R e^{\gamma_E})} S(\omega_L,\omega_R,\mu)\,. \tag{3.1}$$

Whereas the soft function is a distribution in the arguments $\omega_{L,R}$, the Laplace-transformed soft function is a regular function of its arguments. The renormalized soft function in Laplace space is obtained from the bare one through multiplication by a UV renormalization factor. We write the relation between the bare and renormalized functions as

$$\tilde{s}(\tau_L,\tau_R,\mu) = \tilde{Z}_S(\tau_L,\tau_R,\epsilon,\mu)\tilde{s}(\tau_L,\tau_R,\epsilon)\,. \tag{3.2}$$

The notation, used throughout the paper, is such that bare and renormalized functions are distinguished through their last argument, which is μ for renormalized functions and ϵ for bare ones, where the dimensional regulator is $\epsilon = (4-d)/2$. On the other hand, in generic expressions such as (1.4), we drop the dependence on μ or ϵ to indicate that the equations can refer equally well to bare or renormalized quantities. The form and explicit results for the renormalization factor $\tilde{Z}_S$ are well known — we collect some of the expressions we need in the analysis below in appendix B.

We now show how to reproduce the NNLO results of [9, 10] for the hemisphere soft function using the factorization formalism from the previous section. We first define the Laplace-transformed component functions as

$$\widetilde{\boldsymbol{\mathcal{H}}}{}^S_m(\{\underline{n}\},\tau_R) = \int_0^\infty d\omega_R\, e^{-\omega_R/(\tau_R e^{\gamma_E})} \boldsymbol{\mathcal{H}}^S_m(\{\underline{n}\},\omega_R) \tag{3.3}$$

and

$$\widetilde{\boldsymbol{\mathcal{S}}}_m(\{\underline{n}\},\tau_L) = \int_0^\infty d\omega_L\, e^{-\omega_L/(\tau_L e^{\gamma_E})} \boldsymbol{\mathcal{S}}_m(\{\underline{n}\},\omega_L)\,. \tag{3.4}$$

JHEP12(2016)018

The functions with different numbers of hard partons mix under renormalization. Following [20], we define the renormalized hard functions according to

$$\widetilde{\boldsymbol{\mathcal{H}}}_m^S(\{\underline{n}\},\tau_R,\epsilon) = \sum_{l=0}^{m} \widetilde{\boldsymbol{\mathcal{H}}}_l^S(\{\underline{n}\},\tau_R,\mu)\, \widetilde{\boldsymbol{\mathcal{Z}}}_{lm}(\{\underline{n}\},\tau_R,\epsilon,\mu)\,. \tag{3.5}$$

This equation states that lower-multiplicity hard functions absorb some of the divergences of the higher-point functions. This is familiar from fixed-order computations, where virtual corrections to lower-point amplitudes need to be combined with real-emission contributions.

Combined with the fact that the UV divergences for the hemisphere soft function are removed by the renormalization factor $\tilde{Z}_S$, the renormalized soft functions can be written as

$$\widetilde{\boldsymbol{\mathcal{S}}}_{l+1}(\{\underline{n}\},\tau_L,\mu) = \sum_{m=l}^{\infty} \Big[\tilde{Z}_S(\tau_L,\tau_R,\epsilon,\mu)\, \widetilde{\boldsymbol{\mathcal{Z}}}_{lm}(\{\underline{n}\},\tau_R,\epsilon,\mu)\Big] \hat{\otimes}\, \widetilde{\boldsymbol{\mathcal{S}}}_{m+1}(\{\underline{n}\},\tau_L,\epsilon)\,. \tag{3.6}$$

The peculiar index structure arises because in the factorization theorem (1.4) for the hemisphere soft function, the hard function $\widetilde{\boldsymbol{\mathcal{H}}}_m^S$ multiplies $\widetilde{\boldsymbol{\mathcal{S}}}_{m+1}$. This relation has several non-trivial features. First of all, it implies that higher-multiplicity soft functions enter the renormalization of lower-multiplicity ones. The higher-m functions depend on additional directions which need to be integrated over. This integral over unresolved directions is indicated by the symbol $\hat{\otimes}$. Both $\tilde{Z}_S$ and the $\widetilde{\boldsymbol{\mathcal{Z}}}_{lm}$ depend on the hard scale τ_R. It is a non-trivial cross check on our results that the renormalized soft function depends only on τ_L, as it must.

The Laplace-transformed hemisphere soft function satisfies a factorization formula of the same form as (1.4). In order to verify it to NNLO, we first define expansion coefficients of the bare and renormalized functions as

$$\tilde{s}(\tau_L,\tau_R,\epsilon) = \sum_{n=0}^{\infty} \left(\frac{\alpha_0}{4\pi}\right)^n \tilde{s}^{(n)}(\tau_L,\tau_R,\epsilon)\,, \tag{3.7}$$

$$\tilde{s}(\tau_L,\tau_R,\mu) = \sum_{n=0}^{\infty} \left(\frac{\alpha_s}{4\pi}\right)^n \tilde{s}^{(n)}(\tau_L,\tau_R,\mu)\,, \tag{3.8}$$

and similarly for the component functions $\widetilde{\boldsymbol{\mathcal{H}}}_m^S$ and $\widetilde{\boldsymbol{\mathcal{S}}}_m$. Our definitions are such that bare coupling constant in d-dimensions is written as $\alpha_0\tilde{\mu}^{2\epsilon}$, where $\tilde{\mu}^2 = \mu^2 e^{\gamma_E}/(4\pi)$ is chosen to obtain results in the $\overline{\text{MS}}$ scheme. The renormalized coupling constant $\alpha_s \equiv \alpha_s(\mu)$ is related to the dimensionless coupling constant α_0 as $\alpha_s = Z_\alpha^{-1}\alpha_0$, where

$$Z_\alpha = 1 - \frac{\alpha_s}{4\pi}\frac{\beta_0}{\epsilon} + \dots\,; \qquad \beta_0 = \frac{11}{3}C_A - \frac{4}{3}T_F n_f\,. \tag{3.9}$$

Writing out the contributions to the factorization theorem (1.4) to first order, we obtain

$$\begin{aligned}\tilde{s}^{(1)}(\tau_L,\tau_R) = {}& \big\langle \widetilde{\boldsymbol{\mathcal{H}}}_0^{S(0)}(\tau_R)\, \widetilde{\boldsymbol{\mathcal{S}}}_1^{(1)}(\{n\},\tau_L)\big\rangle + \big\langle \widetilde{\boldsymbol{\mathcal{H}}}_0^{S(1)}(\tau_R)\, \widetilde{\boldsymbol{\mathcal{S}}}_1^{(0)}(\{n\},\tau_L)\big\rangle \\ & + \big\langle \widetilde{\boldsymbol{\mathcal{H}}}_1^{S(1)}(\{n_1\},\tau_R) \otimes \widetilde{\boldsymbol{\mathcal{S}}}_2^{(0)}(\{n,n_1\},\tau_L)\big\rangle\,,\end{aligned} \tag{3.10}$$

JHEP12(2016)018

where we have made explicit that the two terms on the first line have no angular dependence, so that the convolution of functions reduces to simple product. Higher-multiplicity terms do not arise since the hard functions are suppressed, $\widetilde{\boldsymbol{\mathcal{H}}}_m^S \sim \alpha_s^m$. The formula simplifies further after noting that perturbative corrections to the zero-emission hard function are scaleless and vanish in dimensional regularization, so that $\widetilde{\boldsymbol{\mathcal{H}}}_0^S(\tau_R, \epsilon) = \mathbf{1}$. Furthermore the leading order soft functions $\widetilde{\boldsymbol{\mathcal{S}}}_m^{(0)} = \mathbf{1}$ are trivial since the Wilson lines reduce to unit matrices at leading order. Suppressing the dependence on the arguments, the one-loop result reads

$$\tilde{s}^{(1)}(\tau_L, \tau_R) = \langle \widetilde{\boldsymbol{\mathcal{S}}}_1^{(1)} \rangle + \langle \widetilde{\boldsymbol{\mathcal{H}}}_1^{S(1)} \otimes \mathbf{1} \rangle \,. \tag{3.11}$$

Applying the same simplifications, the NNLO coefficient reads

$$\tilde{s}^{(2)}(\tau_L, \tau_R) = \langle \widetilde{\boldsymbol{\mathcal{S}}}_1^{(2)} \rangle + \langle \widetilde{\boldsymbol{\mathcal{H}}}_1^{S(1)} \otimes \widetilde{\boldsymbol{\mathcal{S}}}_2^{(1)} \rangle + \langle \widetilde{\boldsymbol{\mathcal{H}}}_1^{S(2)} \otimes \mathbf{1} \rangle + \langle \widetilde{\boldsymbol{\mathcal{H}}}_2^{S(2)} \otimes \mathbf{1} \rangle \,. \tag{3.12}$$

In the following, we give explicit results for the ingredients in these two formulas. We can evaluate equations (3.11) and (3.12) using bare ingredients or renormalized ones. In the main text, we will work with renormalized quantities, but in appendix B we repeat the computation using bare ones.

3.1 Soft functions

As we stressed at the end of section 2, the soft functions are trivially related to the coft functions $\boldsymbol{\mathcal{U}}_m$ relevant for narrow-jet cross sections defined in [20, 21]. Indeed, after setting the cone-angle parameter $\delta = 1$, the soft function for the left-jet mass (2.11) is identical to the coft function

$$\widetilde{\boldsymbol{\mathcal{S}}}_m(\{\underline{n}\}, \tau_L) = \widetilde{\boldsymbol{\mathcal{U}}}_m(\{\underline{n}\}, \tau_L) \,. \tag{3.13}$$

As discussed after (2.11), for the case of the hemisphere soft function the first reference vector must be set equal to n^μ, see (2.8), because the Wilson line along the n-direction is present in the original hemisphere soft function (2.2) and only the remaining $(m-1)$ Wilson lines arise from hard partons. To be able to use our results in both cases, we will give results for the left-jet mass case.

The one-loop soft function is a sum over dipoles

$$\boldsymbol{\mathcal{S}}_m(\{\underline{n}\}, \omega_L, \epsilon) = \mathbf{1} - g_s^2\, \tilde{\mu}^{2\epsilon} \sum_{(ij)} \boldsymbol{T}_i \cdot \boldsymbol{T}_j \int \frac{d^{d-1}k}{(2\pi)^{d-1} 2E_k} \frac{n_i \cdot n_j}{n_i \cdot k\, n_j \cdot k} \\ \theta(n \cdot k - \bar{n} \cdot k) \delta(\omega_L - \bar{n} \cdot k) + \dots \,, \tag{3.14}$$

where the summation of (ij) goes over all unordered pairs, and we can restrict the soft emission to the left hemisphere because the contribution from the right hemisphere is a scaleless integral.

It is useful to separate out the dipoles involving the left-Wilson line $\boldsymbol{S}_0(\bar{n})$ and write the one-loop coefficient of the function in Laplace space in the general form

$$\widetilde{\boldsymbol{\mathcal{S}}}_m^{(1)}(\{\underline{n}\}, \tau_L) = -\sum_i \boldsymbol{T}_0 \cdot \boldsymbol{T}_i\, u(\hat{\theta}_i, \tau_L) - \frac{1}{2} \sum_{[ij]} \boldsymbol{T}_i \cdot \boldsymbol{T}_j\, v(\hat{\theta}_i, \hat{\theta}_j, \phi_i - \phi_j, \tau_L) \,, \tag{3.15}$$

JHEP12(2016)018

where the summation of $[ij]$ goes over all unordered pairs with $i,j \neq 0$. Here ϕ_i is the angle of the n_i in the plane transverse to the thrust direction and

$$\hat{\theta}_i = \sqrt{\frac{n\cdot n_i}{\bar{n}\cdot n_i}} = \tan\left(\frac{\theta_i}{2}\right) \tag{3.16}$$

parameterizes the angle with respect to the thrust axis. Since the terms in the first sum depend only on a single reference vector n_i, the coefficient $u(\hat{\theta}_i, \tau_L)$ is a function of the corresponding angle. The result for the renormalized coefficient functions can be obtained from the results for the coft function $\widetilde{\boldsymbol{\mathcal{U}}}_2$ given in [20]. We find

$$u(\hat{\theta}_1, \tau_L, \mu) = -4\ln^2\left(\frac{\tau_L}{\mu}\right) - 4\ln\left(\frac{\tau_L}{\mu}\right)\ln\left(1-\hat{\theta}_1^2\right) + f_0\left(\hat{\theta}_1\right) - \frac{\pi^2}{2}\,, \tag{3.17}$$

$$\begin{aligned} v(\hat{\theta}_1, \hat{\theta}_2, \Delta\phi, \tau_L, \mu) &= 2g_0\Big(\hat{\theta}_1, \hat{\theta}_2, \Delta\phi\Big) + f_0\Big(\hat{\theta}_1\Big) - f_0\left(\hat{\theta}_2\right) \\ &\quad + 4\ln\left(\frac{1+\hat{\theta}_1^2\hat{\theta}_2^2 - 2\hat{\theta}_1\hat{\theta}_2\cos\Delta\phi}{(1-\hat{\theta}_1^2)(1-\hat{\theta}_2^2)}\right)\ln\frac{\tau_L}{\mu}\,. \end{aligned} \tag{3.18}$$

The function u involves double logarithms due to a collinear singularity from the region where the emission is collinear to $\bar{n}$. The function v on the other hand, describes an exchange between Wilson lines in the right hemisphere. Since the gluon is emitted to the left, this function does not suffer from a collinear singularity. The auxiliary functions f_0 and g_0 were given in [20] and read

$$f_0(\hat{\theta}_1) = -2\ln^2(1-\hat{\theta}_1^2) - 2\mathrm{Li}_2(\hat{\theta}_1^2)\,, \tag{3.19}$$

$$\begin{aligned} g_0(\hat{\theta}_1, \hat{\theta}_2, \pi) &= -\ln^2(1-\hat{\theta}_1^2) - 3\ln^2(1-\hat{\theta}_2^2) + 2\left[\ln(1-\hat{\theta}_1^2) + \ln(1-\hat{\theta}_2^2)\right]\ln(1+\hat{\theta}_1\hat{\theta}_2) \\ &\quad - 2\,\mathrm{Li}_2(\hat{\theta}_2^2) + 2\,\mathrm{Li}_2(-\hat{\theta}_1\hat{\theta}_2) - 2\,\mathrm{Li}_2\left(-\frac{\hat{\theta}_1^2+\hat{\theta}_1\hat{\theta}_2}{1-\hat{\theta}_1^2}\right) - 2\,\mathrm{Li}_2\left(-\frac{\hat{\theta}_2^2+\hat{\theta}_1\hat{\theta}_2}{1-\hat{\theta}_2^2}\right). \end{aligned}$$

For the function $\widetilde{\boldsymbol{\mathcal{S}}}_2$, it is sufficient to consider the case $\Delta\phi = \pi$ due to transverse momentum conservation in the hard function $\widetilde{\boldsymbol{\mathcal{H}}}_2^S$. For the hemisphere soft function in (1.4), we set $n_1 = n$ so that we only need

$$g_0(0, \hat{\theta}, \Delta\phi) = -2\ln^2(1-\hat{\theta}^2)\,. \tag{3.20}$$

To evaluate the color structure for the soft function with three legs explicitly, one can use the relation

$$-2\,\boldsymbol{T}_0\cdot\boldsymbol{T}_1 = \boldsymbol{T}_0^2 + \boldsymbol{T}_1^2 - \boldsymbol{T}_2^2 \tag{3.21}$$

which follows from color conservation $\sum_{i=0}^2 \boldsymbol{T}_i = 0$ together with $\boldsymbol{T}_i^2 = C_i\,\mathbf{1}$, where C_i is the quadratic Casimir of the relevant representation, $C_q = C_F$ and $C_g = C_A$.

For $\widetilde{\boldsymbol{\mathcal{S}}}_1$ in the left-jet case, we can set $n_1 = n$ ($\theta_1 = 0$) since the hard function will enforce that the single hard parton must fly along the thrust axis. For completeness, we reproduce the two-loop result for this function given in [20]. Using relation (3.13) we have

$$\langle\widetilde{\boldsymbol{\mathcal{S}}}_1(\{n\}, \tau_L, \mu)\rangle = 1 + \frac{C_F\alpha_s}{4\pi}\left(-4L_L^2 - \frac{\pi^2}{2}\right) + \left(\frac{\alpha_s}{4\pi}\right)^2\left(C_F^2\,u_1^F + C_F C_A\,u_1^A + C_F T_F n_f\,u_1^f\right), \tag{3.22}$$

JHEP12(2016)018

where $L_L = \ln(\tau_L/\mu)$ and

$$
\begin{aligned}
u_1^F &= 8L_L^4 + 2\pi^2 L_L^2 + \frac{\pi^4}{8}\,, \\
u_1^A &= \frac{88L_L^3}{9} - \frac{268L_L^2}{9} + \left(\frac{844}{27} - \frac{22\pi^2}{9} - 28\zeta_3\right)L_L - \frac{836}{81} - \frac{1139\pi^2}{108} - \frac{187\zeta_3}{9} + \frac{4\pi^4}{5}\,, \\
u_1^f &= -\frac{32L_L^3}{9} + \frac{80L_L^2}{9} + \left(-\frac{296}{27} + \frac{8\pi^2}{9}\right)L_L - \frac{374}{81} + \frac{109\pi^2}{27} + \frac{68\zeta_3}{9}\,.
\end{aligned}
\tag{3.23}
$$

The renormalization of the soft function is quite non-trivial since higher-multiplicity function mix into lower ones, see (3.6). It is therefore interesting to test that the renormalization factor, obtained from absorbing the divergences of the hard functions, indeed renders the soft functions finite. For the case of narrow-jet cross sections, this was verified in [20]. Since we work with different hard functions in the present case, it is an important but somewhat tedious exercise to show that one recovers the same soft function after performing the renormalization. We have checked that this is the case — the details can be found in appendix C.

3.2 Hard functions

Since $\widetilde{\boldsymbol{\mathcal{H}}}_0^S(\tau_R,\epsilon) = \mathbf{1}$ is trivial, the first nontrivial hard function is $\widetilde{\boldsymbol{\mathcal{H}}}_1^S(\{n_1\},\tau_R,\epsilon)$, which arises from the emission of a single hard gluon from the Wilson-line operator in (2.4). The leading contribution to this hard function is given by

$$
\begin{aligned}
\frac{\alpha_s}{4\pi}\widetilde{\boldsymbol{\mathcal{H}}}_1^{S(1)}(\{n_1\},\tau_R,\epsilon) = \frac{2C_F g_s^2\,\tilde{\mu}^{2\epsilon}}{(2\pi)^{2-2\epsilon}}\int_0^\infty d\omega_R \int dE_1 E_1^{1-2\epsilon}\frac{n\cdot\bar{n}}{n\cdot p_1 \bar{n}\cdot p_1}\theta(\bar{n}\cdot p_1 - n\cdot p_1) \\
\times e^{-\omega_R/(\tau_R e^{\gamma_E})}\delta(\omega_R - n\cdot p_1)\mathbf{1}\,.
\end{aligned}
\tag{3.24}
$$

The light-cone vector n_1 appearing as an argument in the hard function is related to the gluon momentum according to $p_1^\mu = E_1 n_1^\mu$. We parameterize this vector in d-dimensions as $n_1 = (1,0,\ldots,\cos\theta_1)$, so that the theta-function constraint in (3.24) gives support to the hard function only in the region $0 < \cos\theta_1 < 1$, that is, when the gluon is in the right hemisphere. After integrating over E_1 and ω_R and performing the trivial angular integrations, we are left with an angular convolution in θ_1. It is convenient to instead use the angular variable $\hat{\theta}_1$ defined in (3.16) and write

$$
\begin{aligned}
\widetilde{\boldsymbol{\mathcal{H}}}_1^{S(1)}(\{n_1\},\tau_R,\epsilon)\otimes\widetilde{\boldsymbol{\mathcal{S}}}_2^{(1)}(\{n_1\},\tau_L,\epsilon) &= \int\frac{d\Omega(n_1)}{4\pi}\widetilde{\boldsymbol{\mathcal{H}}}_1^{S(1)}(\{n_1\},\tau_R,\epsilon)\,\widetilde{\boldsymbol{\mathcal{S}}}_2^{(1)}(\{n_1\},\tau_L,\epsilon) \\
&= \int_0^1 d\hat{\theta}_1\widetilde{\boldsymbol{\mathcal{H}}}_1^{S(1)}(\hat{\theta}_1,\tau_R,\epsilon)\widetilde{\boldsymbol{\mathcal{S}}}_2^{(1)}(\hat{\theta}_1,\tau_L,\epsilon)\,,
\end{aligned}
\tag{3.25}
$$

where we have absorbed the trivial part of the angular integration into $\widetilde{\boldsymbol{\mathcal{H}}}_1^{S(1)}(\hat{\theta}_1,\tau_R,\epsilon)$. For the bare hard function at NLO, we obtain the simple result

$$
\widetilde{\boldsymbol{\mathcal{H}}}_1^{S(1)}(\hat{\theta}_1,\tau_R,\epsilon) = 8C_F\left(\frac{\mu}{\tau_R}\right)^{2\epsilon}\frac{e^{-\epsilon\gamma_E}\Gamma(-2\epsilon)}{\Gamma(1-\epsilon)}\,\hat{\theta}_1^{-1+2\epsilon}\,\mathbf{1}\,.
\tag{3.26}
$$

JHEP12(2016)018

The hard function is thus a distribution in the angle $\hat{\theta}_1$, in contrast the soft function which is regular for $\hat{\theta}_1 \to 0$. To obtain the renormalized hard function, one uses the identity

$$\hat{\theta}_1^{-1+2\epsilon} = \frac{1}{2\epsilon}\delta(\hat{\theta}_1) + \left[\frac{1}{\hat{\theta}_1}\right]_+ + 2\epsilon\left[\frac{\ln\hat{\theta}_1}{\hat{\theta}_1}\right]_+ + \dots . \tag{3.27}$$

The renormalized one-loop function is given by

$$\widetilde{\boldsymbol{\mathcal{H}}}_1^{S(1)}(\hat{\theta}_1, \tau_R, \mu) = \widetilde{\boldsymbol{\mathcal{H}}}_1^{S(1)}(\hat{\theta}_1, \tau_R, \epsilon) - \widetilde{\boldsymbol{\mathcal{H}}}_0^{S(0)}(\tau_R, \epsilon)\widetilde{\boldsymbol{\mathcal{Z}}}_{01}^{(1)}(\hat{\theta}_1, \tau_R, \epsilon, \mu) \tag{3.28}$$

$$= \widetilde{\boldsymbol{\mathcal{H}}}_1^{S(1)}(\hat{\theta}_1, \tau_R, \epsilon) - \widetilde{\boldsymbol{\mathcal{Z}}}_{01}^{(1)}(\hat{\theta}_1, \tau_R, \epsilon, \mu)\,. \tag{3.29}$$

At this order, renormalization is equivalent to dropping the divergences in the bare function. Doing so leaves the finite result

$$\widetilde{\boldsymbol{\mathcal{H}}}_1^{S(1)}(\hat{\theta}_1, \tau_R, \mu) = C_F\left\{\left(-4L_R^2 - \frac{\pi^2}{2}\right)\delta(\hat{\theta}_1) + 8L_R\left[\frac{1}{\hat{\theta}_1}\right]_+ - 8\left[\frac{\ln\hat{\theta}_1}{\hat{\theta}_1}\right]_+\right\}\mathbf{1}\,, \tag{3.30}$$

with $L_R = \ln(\tau_R/\mu)$.

Finally, we also need $\widetilde{\boldsymbol{\mathcal{H}}}_1^{S(2)}$, the one-loop correction to the one-emission function, as well as the leading-order two-emission function $\widetilde{\boldsymbol{\mathcal{H}}}_2^{S(2)}$. Both of these are $\mathcal{O}(\alpha_s^2)$ corrections. Rather than computing the full functions, it is sufficient to obtain the angular convolution of these functions with the trivial leading-order soft functions. The bare results for these can be extracted from the computations in [9, 10] and are given in appendix B. After renormalization one obtains

$$\begin{aligned}
&\left\langle\left[\widetilde{\boldsymbol{\mathcal{H}}}_1^{S(2)}(\{\underline{n}\}, \tau_R, \mu) + \widetilde{\boldsymbol{\mathcal{H}}}_2^{S(2)}(\{\underline{n}\}, \tau_R, \mu)\right]\otimes\mathbf{1}\right\rangle = C_F^2\left[8L_R^4 + 2\pi^2 L_R^2 + \frac{\pi^4}{8}\right] \\
&+ C_A C_F\left[\frac{88}{9}L_R^3 - \frac{268}{9}L_R^2 + \left(\frac{772}{27} + \frac{22\pi^2}{3} - 20\zeta_3\right)L_R - \frac{1196}{81} - \frac{67\pi^2}{12} + \frac{17\pi^4}{45} - \frac{319\zeta_3}{9}\right] \\
&+ C_F T_F n_f\left[-\frac{32}{9}L_R^3 + \frac{80}{9}L_R^2 - \left(\frac{152}{27} + \frac{8\pi^2}{3}\right)L_R + \frac{238}{81} + \frac{5\pi^2}{3} + \frac{116\zeta_3}{9}\right],
\end{aligned} \tag{3.31}$$

as is shown in appendix C.

3.3 Renormalized results to NNLO

Using (3.22) and (3.30), we immediately obtain the renormalized hemisphere soft function at NLO, which is given by

$$\tilde{s}^{(1)}(\tau_L, \tau_R, \mu) = \langle\widetilde{\boldsymbol{\mathcal{S}}}_1^{(1)}\rangle + \langle\widetilde{\boldsymbol{\mathcal{H}}}_1^{S(1)}\otimes\mathbf{1}\rangle = C_F\left(-4L_L^2 - 4L_R^2 - \pi^2\right). \tag{3.32}$$

We observe that after the substitution $\tau_R \to \tau_L$, the hard function contribution, given by the coefficient of the delta-function term in (3.30), agrees with the soft function contribution given in (3.22). This is easily understood since both arise from the same Wilson line matrix element and the single emission is always left for the soft function and right in the case of the hard function. This simple symmetry is no longer present at the two-loop level, since soft gluons can radiate to the right, while hard partons cannot enter the left hemisphere.

JHEP12(2016)018

To obtain the NNLO result, we also need the convolution of $\widetilde{\boldsymbol{\mathcal{H}}}_1^S$ with the one-loop soft function. It is easy to show that

$$\left\langle \widetilde{\boldsymbol{\mathcal{H}}}_1^{S(1)}(\hat{\theta}_1,\tau_R,\mu)\otimes\widetilde{\boldsymbol{\mathcal{S}}}_2^{(1)}(\hat{\theta}_1,\tau_L,\mu)\right\rangle = C_F^2\left[16L_L^2L_R^2+2\pi^2L_L^2+2\pi^2L_R^2+\frac{\pi^4}{4}\right] + C_AC_F\left[\frac{8\pi^2}{3}L_LL_R+8\zeta_3(L_L-2L_R)-\frac{\pi^4}{45}\right]. \tag{3.33}$$

With the final ingredient in place, we can now evaluate (3.12) by adding (3.22), (3.31) and (3.33). Explicitly, we have

$$\begin{aligned}\tilde{s}^{(2)}(\tau_L,\tau_R,\mu) = {}& C_F^2\frac{1}{2}\left[4L_L^2+4L_R^2+\pi^2\right]^2 + C_FC_A\left[\frac{88}{9}\left(L_L^3+L_R^3\right)-\frac{268}{9}\left(L_L^2+L_R^2\right)\right.\\ &+\frac{8}{3}\pi^2L_LL_R+\left(\frac{844}{27}-\frac{22\pi^2}{9}-20\zeta_3\right)L_L+\left(\frac{772}{27}+\frac{22\pi^2}{3}-36\zeta_3\right)L_R\\ &\left.-\frac{2032}{81}-\frac{871\pi^2}{54}-\frac{506\zeta_3}{9}+\frac{52\pi^4}{45}\right]+C_FT_Fn_f\left[-\frac{32}{9}\left(L_L^3+L_R^3\right)+\frac{80}{9}\left(L_L^2+L_R^2\right)\right.\\ &\left.-\left(\frac{296}{27}-\frac{8\pi^2}{9}\right)L_L-\left(\frac{152}{27}+\frac{8\pi^2}{3}\right)L_R-\frac{136}{81}+\frac{154\pi^2}{27}+\frac{184\zeta_3}{9}\right].\end{aligned} \tag{3.34}$$

This result is equivalent to a result for the integrated soft function given in [9], and to a position-space expression given in [10]. In those references the full hemisphere soft function was evaluated, while we directly obtain the function in the limit $\tau_L \ll \tau_R$. The agreement provides a nontrivial check on our factorization formula (1.4). We have performed similar two-loop checks in our earlier work on jet cross sections. However, in that case we could only compare against numerical results from fixed-order event generators. The present case has the advantage that we can compare against the analytical results from [9, 10].

In earlier work on the hemisphere soft function [9, 10, 34], the result was typically written in the form

$$\widetilde{s}(\tau_L,\tau_R,\mu) = \widetilde{s}_\mu(\tau_L,\mu)\widetilde{s}_\mu(\tau_R,\mu)\widetilde{s}_{\rm ng}(r)\,. \tag{3.35}$$

The non-global remainder $\widetilde{s}_{\rm ng}(r)$ is μ-independent but contains logarithms of the small ratio $r=\tau_L/\tau_R \ll 1$. As it stands, the definition of the non-global piece in (3.35) is not unique. One way to fully specify it is to set $\widetilde{s}_\mu(\tau,\mu)=\sqrt{\widetilde{s}(\tau,\tau,\mu)}$. Dividing out the global pieces from our result, we are then left with

$$\widetilde{s}_{\rm ng}(r) = 1+\left(\frac{\alpha_s}{4\pi}\right)^2\left[C_FC_As_{{\rm ng},A}+C_FT_Fn_fs_{{\rm ng},f}\right], \tag{3.36}$$

where

$$s_{{\rm ng},A} = -\frac{4\pi^2}{3}\ln^2(r)+\left(\frac{4}{3}-\frac{44\pi^2}{9}+8\zeta_3\right)\ln(r)\,, \qquad s_{{\rm ng},f}=\left(-\frac{8}{3}+\frac{16\pi^2}{9}\right)\ln(r)\,.$$

Equally well, we could have defined the global part $\widetilde{s}_\mu(\tau,\mu)$ as the square root of the thrust soft function or the solution of the RG equation for $\widetilde{s}_\mu(\tau,\mu)$ with trivial boundary condition $\widetilde{s}_\mu(\tau,\tau)=1$. With the latter two definitions, the non-global piece would involve constant terms.

JHEP12(2016)018

The reasoning for splitting the soft function into global and non-global parts was that the global piece follows from the RG evolution of the soft function $\widetilde{s}(\tau_L, \tau_R, \mu)$, while the logarithms in the non-global part do not. However, we have completely factorized this soft function in (1.4). Our factorization theorem splits the function into contributions from $\boldsymbol{\mathcal{H}}_m^S$, which live at the scale τ_R, and contributions from $\boldsymbol{\mathcal{S}}_m$, which live at the low scale τ_L. The RG equations for these functions simultaneously resum *all* logarithms in the hemisphere soft function. So from the point of view of our effective theory, the splitting into global and non-global logarithms is artificial. The intricate structure of the logarithms is simply a reflection of the complicated operator structure in the effective theory.

4 Logarithmic corrections to the light-jet mass distribution at NNLO

We can obtain the logarithmic corrections to the light-jet mass distribution from those for the heavy-jet and left-jet mass distributions using (1.5). Since the NNLO corrections to the heavy-jet distribution are known, we first give new results for the NNLO corrections to the left-jet mass, before converting them into results for the light-jet mass and comparing with numerical results from event generators at the end of the section.

The factorization theorem for the left-jet mass distribution was given in (1.6). It is again convenient to work in Laplace space since the convolution with the jet function turns into an ordinary product. Introducing the Laplace transformation as in (3.1) the cross section becomes

$$\tilde{\sigma}(\tau_L) = \sum_{i=q,\bar{q},g} \tilde{j}_i(\tau_L Q) \sum_{m=1}^{\infty} \left\langle \boldsymbol{\mathcal{H}}_m^i(\{\underline{n}\}, Q) \otimes \widetilde{\boldsymbol{\mathcal{S}}}_m(\{\underline{n}\}, \tau_L) \right\rangle . \tag{4.1}$$

The Laplace-transformed jet functions $\tilde{j}_i$ are the standard inclusive jet functions, which are well known. The soft functions are the same as the ones for the hemisphere soft case and were given in section 3.1. This leaves us with a computation of the relevant hard functions and the evaluation of the angular integrals over the directions of the reference vectors.

The definition of the hard functions $\boldsymbol{\mathcal{H}}_m^i$ for the left-jet mass, given in (2.10), involves matrix elements with a single hard parton of flavor $i = q, \bar{q}, g$ on the left and m hard partons on the right. The $m = 1$ hard functions have the form

$$\boldsymbol{\mathcal{H}}_1^q(\hat{\theta}_1, Q, \mu) = \boldsymbol{\mathcal{H}}_1^{\bar{q}}(\hat{\theta}_1, Q, \mu) = \frac{\sigma_0}{2} \delta(\hat{\theta}_1) H(Q^2, \mu) \mathbf{1} , \tag{4.2}$$

where σ_0 is the Born cross section for $\gamma^* \to q\bar{q}$ decay, given in d-dimensions by

$$\sigma_0 = 3\, \alpha\, Q_f^2\, Q \frac{(4\pi)^\epsilon\, \Gamma(2-\epsilon)}{\Gamma(2-2\epsilon)} \left(\frac{\mu}{Q}\right)^{2\epsilon} , \tag{4.3}$$

with $\alpha = e^2/(4\pi)$ the fine structure constant and Q_f the charge of the quark flavor q. Moreover, $H(Q^2, \mu)$ is the standard dijet hard function present also in (1.3), and the δ-function in the angle arises because momentum conservation enforces that $n_1 = n$. The factor $1/2$ is present because it is arbitrary whether we label the quark or anti-quark as being in the left hemisphere, so the two situations are averaged over.

JHEP12(2016)018

We also need the hard functions for the case of two hard partons in the right hemisphere. For the case of a quark-jet in the left hemisphere, we have

$$\boldsymbol{\mathcal{H}}_2^{q(1)}(\hat{\theta}_1,\hat{\theta}_2,\Delta\phi,Q,\epsilon) = 2\sigma_0 C_F \left(\frac{\mu}{Q}\right)^{2\epsilon} \frac{e^{\epsilon\gamma_E}}{\Gamma(1-\epsilon)} \hat{\theta}_1^{-1-2\epsilon}\hat{\theta}_2^{-2\epsilon} \left(\hat{\theta}_1+\hat{\theta}_2\right)^{-3+2\epsilon} \left(1-\hat{\theta}_1\hat{\theta}_2\right)^{-2\epsilon} \times \left[2\hat{\theta}_2\left(1-\hat{\theta}_1^2\right)\left(1-\hat{\theta}_1\hat{\theta}_2\right)\left(\hat{\theta}_1+\hat{\theta}_2\right)+(1-\epsilon)\hat{\theta}_1^2\left(1+\hat{\theta}_2^2\right)^2\right]\delta(\Delta\phi-\pi)\mathbf{1}\,, \tag{4.4}$$

where $\hat{\theta}_1$ is the anti-quark angle and $\hat{\theta}_2$ the one of the gluon. Momentum conservation enforces $\Delta\phi = \phi_2 - \phi_1 = \pi$, which is why we only computed the soft function for this configuration. The thrust-axis constraint imposes the conditions

$$\sqrt{1+\hat{\theta}_1^2} > \hat{\theta}_1+\hat{\theta}_2\,, \qquad\qquad \sqrt{1+\hat{\theta}_2^2} > \hat{\theta}_1+\hat{\theta}_2\,, \tag{4.5}$$

on the angular integration region, which can be added as θ functions to (4.4). This constraint implies in particular that the smaller of the two angles $\hat{\theta}_1$ and $\hat{\theta}_2$ must be less than $1/\sqrt{3}$, which corresponds to a 60° angle from the thrust axis. When the limit is reached the three partons are in a symmetric configuration and have all the same energy. If the angle becomes larger the thrust axis flips, since it always points in the direction of the most energetic parton in a three-parton configuration. For $\epsilon \to 0$, the function $\boldsymbol{\mathcal{H}}_2^q$ has overlapping divergences when the angles $\hat{\theta}_1$ and $\hat{\theta}_2$ go to zero simultaneously. To treat these, one splits the angular integration into two sectors $\hat{\theta}_1 < \hat{\theta}_2$ and $\hat{\theta}_1 > \hat{\theta}_2$ and then parametrizes $\hat{\theta}_1 = u\,\hat{\theta}_2$ with $u = 0\ldots1$ in the first sector and conversely in the second one. Once the divergences are separated one can expand both functions in ϵ using the identity (3.27) in the appropriate variables. At the one-loop level the renormalized expressions can be obtained by simply dropping the divergences which arise in this expansion.

The second configuration which is relevant is the one where we have a gluon jet on the left and a hard $q\bar{q}$ pair on the right. The hard function for this case reads

$$\boldsymbol{\mathcal{H}}_2^{g(1)}(\hat{\theta}_1,\hat{\theta}_2,\Delta\phi,Q,\epsilon) = 2\sigma_0 C_F \left(\frac{\mu}{Q}\right)^{2\epsilon} \frac{e^{\epsilon\gamma_E}}{\Gamma(1-\epsilon)} \hat{\theta}_1^{-2\epsilon}\hat{\theta}_2^{-2\epsilon} \left(\hat{\theta}_1+\hat{\theta}_2\right)^{-2+2\epsilon} \left(1-\hat{\theta}_1\hat{\theta}_2\right)^{-1-2\epsilon} \left[\left(1+\hat{\theta}_2^4\right)\hat{\theta}_1^2+\left(1+\hat{\theta}_1^4\right)\hat{\theta}_2^2+4\hat{\theta}_2^2\hat{\theta}_1^2-\epsilon\left(\hat{\theta}_1+\hat{\theta}_2\right)^2\left(1-\hat{\theta}_1\hat{\theta}_2\right)^2\right]\delta(\Delta\phi-\pi)\mathbf{1} \tag{4.6}$$

and is subject to the same angular constraints (4.5). This hard function does not suffer from divergences when the angles go to zero, so we can immediately set $\epsilon \to 0$.

To obtain the full NNLO result for the left-hemisphere cross section, we would need also the one-loop corrections to $\boldsymbol{\mathcal{H}}_2^i \otimes \mathbf{1}$ and the three-parton functions $\boldsymbol{\mathcal{H}}_3^i \otimes \mathbf{1}$. However, if we are only interested in the logarithmic terms, we can avoid their computation by setting $\mu = Q$. For this scale choice these functions do not contain any logarithms and we can therefore recover the logarithmic part of the NNLO cross section from

$$\tilde{\sigma}(\tau_L) = 2\,\tilde{j}_q(\tau_L Q,\mu)\left\langle \boldsymbol{\mathcal{H}}_1^q(\{n_1\},Q,\mu)\otimes\widetilde{\boldsymbol{\mathcal{S}}}_1(\{n_1\},\tau_L,\mu)\right\rangle + \sum_{i=q,\bar{q},g}\tilde{j}_i(\tau_L Q,\mu)\left\langle \boldsymbol{\mathcal{H}}_2^i(\{n_1,n_2\},Q,\mu)\otimes\widetilde{\boldsymbol{\mathcal{S}}}_2(\{n_1,n_2\},\tau_L,\mu)\right\rangle + \mathcal{O}(\alpha_s^2 L_L^0)\,, \tag{4.7}$$

JHEP12(2016)018

where the factor 2 in the first line accounts for the identical contribution when the anti-quark is in the left hemisphere. The two-loop result for the soft function $\widetilde{\boldsymbol{\mathcal{S}}}_1$ was given in the previous section in (3.22). The dijet hard function (4.2) and the Laplace-space quark jet function $\tilde{j}_q$ are well known. Explicit two-loop results for both quantities can be found in appendix B of [35]. We can thus immediately evaluate the first line of (4.7) and what remains is the convolution on the second line. Since the functions $\boldsymbol{\mathcal{H}}_2^i$ start at $\mathcal{O}(\alpha_s)$, we need the gluon jet function $\tilde{j}_g$ and the soft function $\widetilde{\boldsymbol{\mathcal{S}}}_2$ only to one-loop order.

We have obtained analytical results for the convolutions of the two-parton functions with the trivial leading-order soft functions

$$\sum_{i=q,\bar{q}} \left\langle \boldsymbol{\mathcal{H}}_2^{i(1)}(\{n_1,n_2\},Q,\mu) \otimes \mathbf{1} \right\rangle = C_F\sigma_0 \Bigg[4\,L_Q^2 - 6\,L_Q + \frac{29}{3} - \frac{3\,\pi^2}{2} - 2\ln^2 2 + \frac{5}{4}\ln 3 - 4\,\mathrm{Li}_2\left(-\frac{1}{2}\right) \Bigg], \tag{4.8}$$

$$\left\langle \boldsymbol{\mathcal{H}}_2^{g(1)}(\{n_1,n_2\},Q,\mu) \otimes \mathbf{1} \right\rangle = C_F\sigma_0 \left[-\frac{1}{6} + \frac{\pi^2}{3} + 2\ln^2 2 - \frac{5}{4}\ln 3 + 4\mathrm{Li}_2\left(-\frac{1}{2}\right) \right], \tag{4.9}$$

where $L_Q = \ln(Q/\mu)$. The appearance of logarithms and polylogarithms in addition to the usual ζ-values is a result of the phase-space constraint (4.5). The result in (4.9) agrees with the quantity r_3 obtained in [24], see (22) in [4]. Putting (4.8) together with the other one-loop ingredients we obtain agreement with the result of [4] also in the quark channel. For the NNLO cross section we need results for the convolutions with the NLO soft function (3.14), which have the form

$$\begin{aligned}
&\sum_{i=q,\bar{q}} \left\langle \boldsymbol{\mathcal{H}}_2^{i(1)}(\{n_1,n_2\},Q,\mu) \otimes \widetilde{\boldsymbol{\mathcal{S}}}_2^{(1)}(\{n_1,n_2\},\tau_L,\mu) \right\rangle = \\
&\qquad C_F^2\sigma_0 \left[\left(-16\,L_Q^2 + 24\,L_Q + M_{q,F}^{(2)}\right) L_L^2 + M_{q,F}^{(1)}\,L_L - 2\pi^2 L_Q^2 + 3\pi^2 L_Q + M_{q,F}^{(0)} \right] \\
&\qquad + C_F C_A \sigma_0 \left[\left(\frac{8\pi^2 L_Q}{3} + M_{q,A}^{(1)} \right) L_L - 16\zeta_3 L_Q + M_{q,A}^{(0)} \right], \qquad (4.10) \\
&\left\langle \boldsymbol{\mathcal{H}}_2^{g(1)}(\{n_1,n_2\},Q,\mu) \otimes \widetilde{\boldsymbol{\mathcal{S}}}_2^{(1)}(\{n_1,n_2\},\tau_L,\mu) \right\rangle = \\
&\qquad C_F^2\sigma_0 \left[M_{g,F}^{(1)} L_L + M_{g,F}^{(0)} \right] + C_F C_A \sigma_0 \left[M_{g,A}^{(2)} L_L^2 + M_{g,A}^{(1)} L_L + M_{g,A}^{(0)} \right]. \qquad (4.11)
\end{aligned}$$

The expressions for the coefficients $M_{g,F}^{(i)}$ and $M_{q,F}^{(i)}$ are lengthy and can be found in the appendix in (D.10).

Putting everything together and inverting the Laplace transformation we then obtain all logarithmic terms in the left-jet mass distribution. The inverse Laplace transformation can be obtained using the simple substitution rules

$$\begin{aligned}
&\ln\frac{\tau_L}{Q} \to \ln\rho_L, \quad \ln^2\frac{\tau_L}{Q} \to \ln^2\rho_L - \frac{\pi^2}{6}, \quad \ln^3\frac{\tau_L}{Q} \to \ln^3\rho_L - \frac{\pi^2}{2}\ln\rho_L + 2\zeta_3, \\
&\ln^4\frac{\tau_L}{Q} \to \ln^4\rho_L - \pi^2\ln^2\rho_L + 8\zeta_3\ln\rho_L + \frac{\pi^4}{60}.
\end{aligned} \tag{4.12}$$

JHEP12(2016)018

Using relation (1.5) together with the known result for the logarithmic terms in the heavy-jet mass distribution [23] we then obtain the light-jet mass distribution. Up to NNLO, it has the general form

$$\frac{1}{\sigma_0}\frac{d\sigma}{d\rho_\ell} = \delta(\rho_l)\left\{1+\left(\frac{\alpha_s}{2\pi}\right)\frac{3C_F}{2}+\left(\frac{\alpha_s}{2\pi}\right)^2 B_\delta\right\}+\left(\frac{\alpha_s}{2\pi}\right)^2\left[\frac{B_+(\rho_l)}{\rho_l}\right]_+ +\cdots . \tag{4.13}$$

Note that at NLO, the distribution is a δ-function since the lighter jet contains only a single parton. A nontrivial light-jet mass distribution first arises from four-particle configurations at NNLO in which each hemisphere contains two partons. The logarithmic terms from these configurations are encoded in the function $B_+(\rho_\ell)$, for which we obtain

$$\begin{aligned}
B_+(\rho) = C_F^2\Bigg[&-4\ln^3\rho-9\ln^2\rho+\left[-\frac{59}{6}+\frac{4\pi^2}{3}+4\ln^2 2-\frac{5\ln 3}{2}+8\,\mathrm{Li}_2\left(-\frac{1}{2}\right)\right]\ln\rho\\
&+\frac{15}{2}+2\pi^2+\frac{809\zeta_3}{6}+\frac{88\ln^3 2}{3}+8\ln 2\ln^2 3+\frac{5\ln^2 3}{2}-24\ln^2 2\ln 3+\frac{27\ln^2 2}{2}\\
&-28\ln 2\ln 3+\frac{487\ln 3}{24}-\frac{20}{3}\pi^2\ln 2-\frac{88\ln 2}{3}+43\,\mathrm{Li}_2\left(-\frac{1}{2}\right)-16\,\mathrm{Li}_2\left(-\frac{1}{2}\right)\ln 3\\
&+96\,\mathrm{Li}_2\left(-\frac{1}{2}\right)\ln 2-8\,\mathrm{Li}_3\left(\frac{3}{4}\right)+176\,\mathrm{Li}_3\left(-\frac{1}{2}\right)-8\,I_2\Bigg]\\
+C_FC_A\Bigg[&\left[\frac{1}{3}-2\pi^2-4\ln^2 2+\frac{5\ln 3}{2}-8\mathrm{Li}_2\left(-\frac{1}{2}\right)\right]\ln\rho-\frac{407}{72}-\frac{13\pi^2}{18}-\frac{389\zeta_3}{3}-\frac{8\ln^3 3}{3}\\
&-52\ln^3 2-12\ln 2\ln^2 3-\frac{15\ln^2 3}{4}+52\ln^2 2\ln 3+\frac{43\ln^2 2}{12}-\frac{11}{2}\ln 2\ln 3\\
&-\frac{917\ln 3}{24}+6\pi^2\ln 2+\frac{212\ln 2}{3}+20\,\mathrm{Li}_3\left(\frac{3}{4}\right)+\frac{235}{6}\,\mathrm{Li}_2\left(-\frac{1}{2}\right)\\
&+24\,\mathrm{Li}_2\left(-\frac{1}{2}\right)\ln 3-88\,\mathrm{Li}_2\left(-\frac{1}{2}\right)\ln 2+16\,\mathrm{Li}_3\left(\frac{1}{3}\right)-112\,\mathrm{Li}_3\left(-\frac{1}{2}\right)-8\,I_1\Bigg]\\
+C_FT_Fn_f\Bigg[&-\frac{13}{9}+\frac{10\pi^2}{9}+\frac{4}{3}\ln^2 2-\frac{5}{6}\ln 3+\frac{8}{3}\,\mathrm{Li}_2\left(-\frac{1}{2}\right)\Bigg].
\end{aligned} \tag{4.14}$$

Due to the uncalculated two-loop constant terms in the hard functions $\boldsymbol{\mathcal{H}}_2$ and $\boldsymbol{\mathcal{H}}_3$, we cannot give the two-loop coefficient B_δ, but the δ-function terms do not contribute to the logarithmic corrections to the light-jet mass distribution. We have verified that the terms involving powers of $\ln\rho$ in (4.14) are in agreement with those implied by the results of [4, 24]. The remaining pieces, on the other hand, are new. As a further check, we have repeated the computation of the logarithmic terms in the cross section using bare instead of renormalized quantities. The logarithms are related to divergences in the individual ingredients in the factorization theorem (1.6). To obtain the logarithmic terms in the cross section we thus insert the divergent bare ingredients together with their associated logarithmic terms into the Laplace-transformed version of (1.6). The divergences cancel and we are left with a logarithmic structure which agrees with (4.14). The details of this computation can be found in appendix D.

JHEP12(2016)018

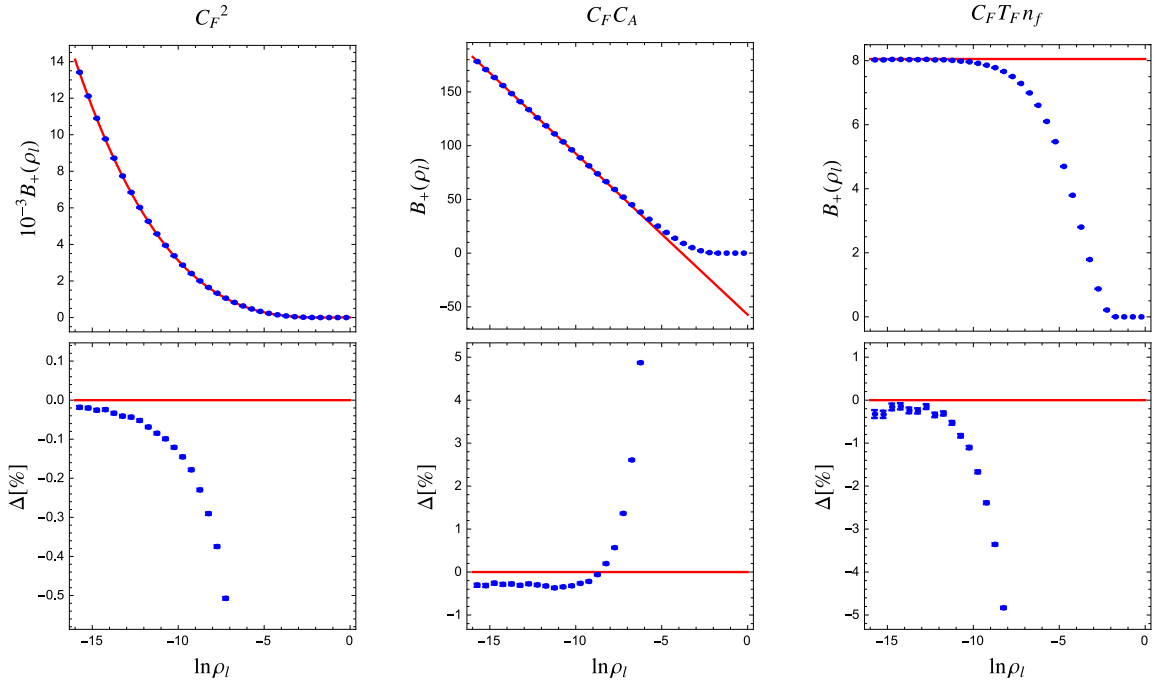

Figure 2. Comparison of our analytic results (solid lines) for the coefficients of the three color structures in the two-loop coefficient $B_+(\rho_l)$ for the light-jet mass distribution with numerical results (points with invisibly small error bars) obtained using the EVENT2 event generator [33]. The two results must agree for small ρ_ℓ. The lower panel shows the relative difference in per cent.

In contrast to the hemisphere soft function, the full analytical result for the light-jet mass distribution is not known, but our result for the coefficient $B_+(\rho_l)$ can be compared to numerical results obtained from running a fixed-order event generator. Since our results are the leading term in the limit $\rho_\ell \to 0$, we need to run the fixed-order code for very small values of ρ_ℓ to suppress higher-power contributions, which makes the numerics delicate. For our comparison, we use EVENT2 [33], which is well suited to study the region of small ρ_ℓ since the phase-space generation can be tuned to focus on this region. We note that the fixed-order result is known even one order higher [36–38] and available in the form of a public code EERAD3 [39]. In order to ensure that the power-suppressed terms are small, we run down to values of $\ln \rho_\ell = -16$. To ensure numerical stability, EVENT2 imposes a cutoff on the invariant mass of parton pairs, and we run the code in quadruple precision to be able to lower the cutoff enough to avoid cutoff effects. Figure 2 shows the EVENT2 result in blue, compared to our analytic result shown as red lines. The statistical error bars on the EVENT2 results are barely visible, since we have generated 300 billion events. The upper panels show that the numerical results indeed approach the leading-power analytic results as the value of ρ_ℓ is lowered. In the lower panel, we show the difference between EVENT2 and the analytic result in per cent, and the two agree to better than half a per cent for low values of ρ_ℓ. However, our statistical uncertainties are even smaller than this and we find residual deviations in all color channels which are larger than the uncertainties. As a cross check, we have performed the same comparison against the well-known analytical result

JHEP12(2016)018

for the heavy-jet mass [23] and find deviations of similar size. Indeed, earlier papers have identified similar numerical issues in several variables [23, 40, 41], so we believe that the remaining deviations are not indicative of a problem in our analytic computation. We have also compared with the results from EERAD3 and from the CoLoRFulNNLO framework [38] but were not able to achieve small enough statistical uncertainties to resolve the difference between EVENT2 and the analytic result.

5 NLL resummation

Our focus has been on the factorization properties of the hemisphere soft function and the light-jet mass distribution. The factorization theorems we derived are important because they enable the resummation of the large logarithms. In our framework, this resummation is achieved by solving the RG evolution equations for the ingredients of the factorization theorem and evolving them to a common reference scale. To perform NLL resummation, which resums the leading non-global logarithms, one needs to evaluate the hard, jet and soft functions at tree level and evolve them using one-loop regular anomalous dimensions, together with the two-loop cusp anomalous dimension. The global part of the light-jet mass distribution at NLL was presented in [24] and the non-global part in the large-N_c limit was computed in [4], but as far as we are aware a numerical result for the NLL resummed single-hemisphere mass distribution including NGLs was never presented in the literature.

The simplest way to obtain the NLL result for the left-jet mass distribution is to choose the factorization scale as $\mu = \mu_h \sim Q$. With this choice, the hard functions do not suffer from large logarithms and at NLL the factorization theorem (1.6) simplifies to

$$\frac{d\sigma}{dM_L^2} = \sigma_0 \int_0^\infty d\omega_L \, J_q(M_L^2 - Q\,\omega_L, \mu_h) \left\langle \boldsymbol{\mathcal{S}}_1(\{n\}, \omega_L, \mu_h) \right\rangle . \tag{5.1}$$

We have used that all higher-order hard functions are suppressed by powers of $\alpha_s(\mu_h)$ and can be neglected at NLL. To obtain the cross section we thus need two ingredients: the resummed quark jet function and the soft function $\boldsymbol{\mathcal{S}}_1(\{n\}, \omega, \mu_h)$ evolved to the hard scale μ_h. This soft function is the same as the NLL resummed result for the hemisphere soft function. Indeed, choosing $\mu = \mu_h$ and integrating ω_R up to a large value $Q \sim \mu_h$ the factorization theorem (1.4) for this quantity at NLL accuracy reduces to

$$\int_0^Q d\omega_R \, S(\omega_L, \omega_R, \mu_h) = \left\langle \boldsymbol{\mathcal{S}}_1(\{n\}, \omega_L, \mu_h) \right\rangle . \tag{5.2}$$

This fact is of course well known and it is for this reason that the non-global logarithms in the light-jet mass are usually studied using the hemisphere soft function. Beyond NLL this simple relationship is no longer valid, because the left-jet mass receives contributions from hard radiation in the right hemisphere.

Before analyzing the soft function further, let us quote the resummed result for the jet function at NLL. Using the Laplace-space technique of [42], one obtains

$$J_q(p^2, \mu_h) = \exp\left[-4S(\mu_j, \mu_h) + 2A_{\gamma^J}(\mu_j, \mu_h)\right] \frac{e^{-\gamma_E \eta_J}}{\Gamma(\eta_J)} \frac{1}{p^2} \left(\frac{p^2}{\mu_j^2}\right)^{\eta_J} , \tag{5.3}$$

where $\eta_J = 2A_\Gamma(\mu_j, \mu_h)$. Explicitly, the Sudakov exponent $S(\mu_j, \mu_h)$ and the single logarithmic function $A_\Gamma(\mu_j, \mu_h)$ are

$$\begin{aligned} S(\mu_j, \mu) &= \frac{\Gamma_0}{4\beta_0^2}\left\{\frac{4\pi}{\alpha_s(\mu_j)}\left(1 - \frac{1}{r} - \ln r\right) + \left(\frac{\Gamma_1}{\Gamma_0} - \frac{\beta_1}{\beta_0}\right)(1 - r + \ln r) + \frac{\beta_1}{2\beta_0}\ln^2 r\right\}, \\ A_\Gamma(\mu_j, \mu) &= \frac{\Gamma_0}{2\beta_0}\ln r\,, \end{aligned} \tag{5.4}$$

where $r = \alpha_s(\mu)/\alpha_s(\mu_j)$. The result for A_{γ^J} is obtained by replacing $\Gamma_0 \to \gamma_0^J$ in $A_\Gamma(\mu_j, \mu)$. The relevant expansion coefficients of the anomalous dimensions and the β-function can be found at the end of appendix B.

The resummed soft function $\langle \boldsymbol{\mathcal{S}}_1(\{n\}, \omega_L, \mu_h)\rangle$ can be obtained by solving the RG equation for the soft functions, which in Laplace space takes the form

$$\frac{d}{d\ln\mu}\,\widetilde{\boldsymbol{\mathcal{S}}}_l(\{\underline{n}\}, \tau, \mu) = \sum_{m=l}^{\infty} \boldsymbol{\Gamma}^S_{lm}(\{\underline{n}\}, \tau, \mu) \,\hat{\otimes}\, \widetilde{\boldsymbol{\mathcal{S}}}_m(\{\underline{n}\}, \tau, \mu)\,. \tag{5.5}$$

Due to the factorization theorem (4.1), the anomalous dimension matrix must take the form

$$\boldsymbol{\Gamma}^S_{lm}(\{\underline{n}\}, \tau, \mu) = 2\,\Gamma_{\rm cusp}\ln\left(\frac{\tau}{\mu}\right)\delta_{lm} + \hat{\boldsymbol{\Gamma}}_{lm}(\{\underline{n}\})\,. \tag{5.6}$$

The cusp piece is diagonal since the τ dependence of the anomalous dimension $\boldsymbol{\Gamma}^S_{lm}$ must cancel against that of the jet function $\tilde{j}_q$ in (4.1). We can thus split the soft functions into a product

$$\widetilde{\boldsymbol{\mathcal{S}}}_l(\{\underline{n}\}, \tau, \mu) = \tilde{S}_G(\tau, \mu)\,\hat{\boldsymbol{\mathcal{S}}}_l(\{\underline{n}\}, \tau, \mu)\,, \tag{5.7}$$

where the global function fulfills the simple RG equation for the cusp part with trivial initial condition $\tilde{S}_G(\tau, \tau) = 1$. In Laplace space this RG equation has the same form as for the jet function and is easily solved. Inverting the Laplace transformation, we obtain

$$S_G(\omega, \mu_h) = \exp\left[2S(\mu_s, \mu_h)\right]\frac{e^{-\gamma_E\eta_S}}{\Gamma(\eta_S)}\,\frac{1}{\omega}\left(\frac{\omega}{\mu_s}\right)^{\eta_S}, \tag{5.8}$$

where $\eta_S = 2A_\Gamma(\mu_h, \mu_s)$. The remaining piece $\hat{\boldsymbol{\mathcal{S}}}_l(\{\underline{n}\}, \tau, \mu)$ in (5.7) has a single logarithmic evolution driven by $\hat{\boldsymbol{\Gamma}}_{lm}(\{\underline{n}\})$, which can be derived from results given in appendix C of [20]. This piece captures the non-global logarithms, through the formal solution

$$\begin{aligned} \langle \hat{\boldsymbol{\mathcal{S}}}_1(\{\underline{n}\}, \tau, \mu_h)\rangle &= \sum_{m=1}^{\infty} \langle \boldsymbol{U}^S_{1m}(\{\underline{n}\}, \mu_s, \mu_h) \,\hat{\otimes}\, \hat{\boldsymbol{\mathcal{S}}}_m(\{\underline{n}\}, \tau, \mu_s)\rangle \\ &= \sum_{m=1}^{\infty} \langle \boldsymbol{U}^S_{1m}(\{\underline{n}\}, \mu_s, \mu_h) \,\hat{\otimes}\, \mathbf{1}\rangle \equiv S_{NG}(\mu_s, \mu_h)\,, \end{aligned} \tag{5.9}$$

where in the second line we used $\hat{\boldsymbol{\mathcal{S}}}_m(\{\underline{n}\}, \tau, \mu_s) = \mathbf{1} + \mathcal{O}(\alpha_s)$, and made explicit that at NLL the quantity $S_{NG}(\mu_s, \mu_h)$ is thus a function of μ_h and μ_s only. The evolution matrix

JHEP12(2016)018

$\boldsymbol{U}^S_{1m}$ evolves the soft function from the low scale μ_s to the high scale μ_h. It is obtained at NLL by exponentiating the one-loop anomalous dimension matrix

$$\boldsymbol{U}^S(\{\underline{n}\},\mu_s,\mu_h) = \mathbf{P}\exp\left[\int_{\mu_s}^{\mu_h}\frac{d\mu}{\mu}\,\hat{\boldsymbol{\Gamma}}(\{\underline{n}\},\mu)\right], \tag{5.10}$$

but due to the angular convolutions and the color structure of the anomalous dimension matrix, deriving an explicit form for the evolution matrix is highly nontrivial. In our paper [20] we demonstrated that in the large-N_c limit the exponentiation of the one-loop anomalous dimension matrix is equivalent to solving the BMS equation. The RG evolution equation (5.5) is also equivalent to a parton-shower equation and this is the way the resummation of the hemisphere soft function was performed in the original paper of Dasgupta and Salam [4], who presented a simple, accurate parameterization of their result. In the future, it will be very interesting to generalize this to higher logarithmic accuracy but for the moment we will simply use their result to obtain a resummed result for the left-jet mass and investigate the size of the leading non-global logarithms in this observable. The parameterization of Dasgupta and Salam has the form

$$S_{\rm NG}(\mu_s,\mu_h) \approx \exp\left(-C_A C_F\frac{\pi^2}{3}\,u^2\frac{1+(au)^2}{1+(bu)^c}\right), \tag{5.11}$$

with

$$u = \frac{1}{\beta_0}\ln\frac{\alpha_s(\mu_s)}{\alpha_s(\mu_h)}, \tag{5.12}$$

where the constants $a = 0.85\,C_A$, $b = 0.86\,C_A$, and $c = 1.33$ were determined by fitting to the parton-shower result.

The resummed result for the soft function in momentum space is then simply the product of the global function with the non-global evolution factor,

$$\langle \boldsymbol{\mathcal{S}}_1(\{\underline{n}\},\omega,\mu_h)\rangle = S_{\rm NG}(\mu_s,\mu_h)S_G(\omega,\mu_h), \tag{5.13}$$

and the final result for the left-jet mass is obtained by convolving the soft function and the jet function. Let us first combine the global piece with the jet function. Integrating also over ρ_L, we obtain

$$\begin{aligned}\Sigma_q(\rho_L) &= \int_0^{\rho_L} d\rho_L' \int_0^{Q\rho_L'} d\omega\, J_q(Q^2\rho_L' - Q\omega,\mu_h)S_G(\omega,\mu_h)\\ &= \exp\left[2S(\mu_s,\mu_h) - 4S(\mu_j,\mu_h) + 2A_{\gamma^J}(\mu_j,\mu_h)\right]\frac{e^{-\gamma_E\eta}}{\Gamma(\eta+1)}\left(\frac{Q^2\rho_L}{\mu_j^2}\right)^{\eta}\left(\frac{Q\mu_s}{\mu_j^2}\right)^{-\eta_S},\end{aligned} \tag{5.14}$$

where $\eta = \eta_J + \eta_S = 2A_\Gamma(\mu_j,\mu_s)$. The integrated left-jet distribution is then obtained as

$$R(\rho_L) = \int_0^{\rho_L} d\rho_L'\frac{1}{\sigma}\frac{d\sigma}{d\rho_L'} = S_{\rm NG}(\mu_s,\mu_h)\Sigma_q(\rho_L), \tag{5.15}$$

where we need to choose $\mu_s \sim \rho_L Q$ and $\mu_h \sim Q$. The quantity Σ_q plays an important role in the coherent branching formalism [43–45], where it arises as an integral over the jet

JHEP12(2016)018

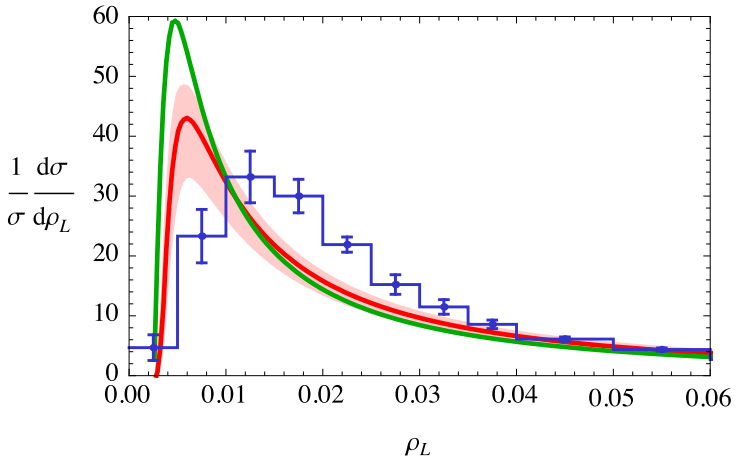

Figure 3. NLL result for the left-jet mass distribution (red curve). The red uncertainty band is obtained from scale variations as explained in the text. The green line is the purely global part of the distribution. In blue we show experimental results from ALEPH [48].

function. We verified that (5.14) indeed reproduces the result for this quantity given in [24] after setting the scales to the default values $\mu_j^2 = \rho_L Q^2$ and $\mu_s = \rho_L Q$. Formula (5.14) shows that the jet function in the coherent-branching formalism also includes the global part of the soft radiation. Our final resummed result (5.15) is therefore fully equivalent to that presented in [4]. Squaring Σ_q, one obtains the integrated heavy-jet mass at NLL:

$$R(\rho_h) = [\Sigma_q(\rho_h)]^2 \,. \tag{5.16}$$

We have checked that using (5.14) in the above result reproduces the resummed result of [23]. Below we will use the result for $R(\rho_h)$ together with relation (1.5) to obtain the light-jet mass from the left-jet mass distribution (5.15).

The result for the resummed left-jet mass distribution (5.1) is shown in figure 3. For our plots, we choose $Q = M_Z$ and $\alpha_s(M_Z) = 0.1181$ [46]. The red line shows the result for the default scale choices, and to estimate its uncertainty, we perform two different scale variations. In particular, we separately vary the hard scale μ_h and the jet scale μ_j by factors of two around the default choices $\mu_h^2 = Q^2$ and $\mu_j^2 = \rho_L Q^2$, and show in the plots the envelope of the two variations. At very low values of ρ_L the spectrum ends because $\mu_s = \rho_L Q$ hits the Landau pole. One could also vary the soft scale, which would shift this end-point and thus generate a larger uncertainty band. The green line in the plot shows the global part of the left jet mass, i.e. the result without including $S_{\rm NG}(\mu_s, \mu_h)$. The difference between the two curves demonstrates that the non-global pieces have an important effect on the distribution. Note that the distributions shown in the plot are obtained from taking the derivative of the resummed cumulant $R(\rho_L)$ in (5.15) with respect to ρ_L. For fixed scales, integrating and differentiating would commute, but we choose the values of the scales in the cumulant and then take the derivative, which is advantageous, as explained in [47]. One benefit is that the spectrum is automatically normalized since $R(\rho_L) \to 1$ for $\rho_L = 1$ (the true upper limit of the spectrum is at a lower value and one often modifies the

JHEP12(2016)018

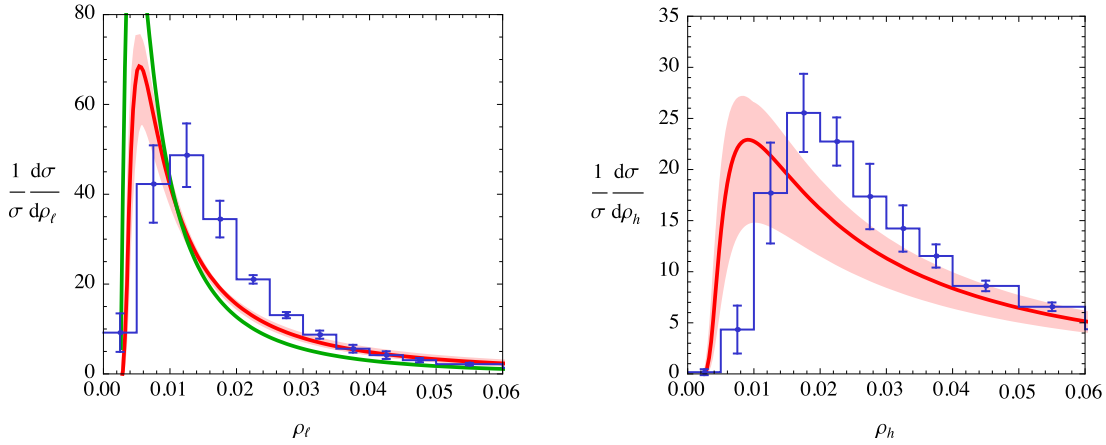

Figure 4. The red bands show the NLL result for the light-jet mass (left) and the heavy-jet mass (right), compared to ALEPH data (blue) [48]. The green line is the purely global part of the light-jet mass distribution and peaks at a value of about 110.

resummation prescription such that the result vanishes beyond the kinematical limit; for simplicity we will not do this here).

Our plots also include experimental results from the ALEPH collaboration [48]. The LEP experiments have measured the light-jet and heavy-jet mass distributions and we have used relation (1.5) to convert their measurements into a result for the left-jet mass, naively adding the uncertainties on the two distributions in quadrature. It is obviously better to directly compare to the experimental result for the individual measurements, which is done in figure 4. The comparison shows that non-perturbative effects, which will shift the peak to the right, are important at low values of ρ_L, where the distribution is large. This is expected since the soft scale is $\mu_s \sim \rho_L Q$ and takes non-perturbative values near the peak, especially for the light-jet mass. To reproduce the data, one would have to include such non-perturbative effects, and should also match to the fixed-order results to get a better description at higher values of ρ_ℓ and ρ_h. For the moment, we will not pursue these issues further. Our goal was to assess whether non-global effects are phenomenologically relevant and our results clearly show that this is indeed the case for the non-global hemisphere event shapes. Studies of leading non-global logarithms were also performed for the more complicated case of high-p_T jet shapes [49, 50]. Also in these observables, the non-global effects are sizeable.

6 Conclusions and outlook

We have studied the factorization of large logarithmic corrections appearing in non-global hemisphere-mass observables at e^+e^- colliders. We focused our analysis on two particular cases: *i.*) the double differential cross section with respect to the left and right hemisphere masses M_L and M_R in the limit where $M_L \ll M_R \ll Q$, and *ii.*) the left-jet mass distribution in the limit where $M_L \ll Q$. Our main result in the first case was the derivation of a factorization formula for the hemisphere soft function $S(\omega_L, \omega_R)$ in the limit $\omega_L \ll \omega_R$,

JHEP12(2016)018

while in the second case we presented a novel factorization formula for the differential cross section itself.

While the specifics of the two cases are slightly different, the ideas behind them are rather general, and indeed for the most part could be adapted from the analysis of cone-jet cross sections in [20]. In particular, the key feature of factorization formulas for such non-global observables is that additional wide-angle emissions of hard partons at each order in perturbation theory build up a tower of multi-Wilson-line operators in the effective field theory. The matrix elements of these operators define multi-Wilson-line soft functions, which appear in angular convolution integrals with their (distribution valued) Wilson coefficients, referred to as multi-parton hard functions.

We confirmed the validity of our factorization formulas through explicit NNLO calculations. For the hemisphere soft function, we showed that our results reproduce the known analytic ones from [9, 10], including all constant and logarithmic pieces appearing in the limit $\omega_L \ll \omega_R$. For the light-jet mass, on the other hand, we obtained only the logarithmically enhanced NNLO corrections, and validated them through numerical comparisons with event generators. In both cases, the main new perturbative results presented here were those for the multi-parton hard functions, since other ingredients appearing in the factorization could be taken from the literature. We calculated these to NLO in the case of the left-jet mass, and to NNLO in the case of the hemisphere soft function, thus providing a non-trivial example at NNLO of the renormalization procedure involving mixing of multi-Wilson-line operators characteristic of non-global observables.

The factorization formulas derived here provide the basis for all-orders resummation of non-global logarithms for these observables. To get an idea of the size of the effects, we have used the known result for the leading non-global logarithms in the hemisphere soft function to obtain the left-jet mass distribution at NLL. We find that the non-global effects, evaluated in the large-N_c limit, are of the same magnitude as other NLL effects. For precision predictions of non-global observables, it would be important to include also higher-logarithmic effects. The necessary ingredients are available: we have computed the one-loop soft functions and hard functions and the relevant two-loop anomalous dimensions can be extracted from the work of [22]. Since one has to exponentiate an infinite-dimensional anomalous dimension matrix, it is not possible to obtain analytic results and the resummation has to be performed numerically. One approach is to incorporate the corrections into the parton-shower framework used to compute the leading logarithmic corrections. It will be interesting to analyze how this can be done in an efficient way and to use our framework to produce precision predictions for non-global observables.

Acknowledgments

We thank Pier Francesco Monni, Matthias Neubert and Lorena Rothen for discussions, and Adam Kardos and Zoltan Trócsányi for sending us results for the light-jet mass obtained using the CoLoRFulNNLO framework. The research of T.B. is supported by the Swiss National Science Foundation (SNF) under grant 200020_165786. The authors thank the ESI Vienna for hospitality and support during early stages of this work.

JHEP12(2016)018

A Absence of leading-power collinear contributions to $S(\omega_L, \omega_R)$

One might expect that left-collinear modes with scaling

$$(n \cdot p_c, \bar{n} \cdot p_c, p_c^\perp) \sim (1, \kappa, \sqrt{\kappa})\, \omega_R \tag{A.1}$$

could contribute to the hemisphere soft function, since they have $\bar{n} \cdot p \sim \omega_L$, as required. The operator definition for the associated leading-power jet function has the form

$$J_c(\omega_L) = \sum_{X_L} \left| \langle X_L | W_{\bar{n}}^\dagger W_n | 0 \rangle \right|^2 \delta\Big(\omega_L - \sum_i \bar{n} \cdot P_L^i\Big)\,, \tag{A.2}$$

where the Wilson lines W_n are built from collinear fields and are invariant under rescaling of the reference vector. The multipole expansion ensures that the left-collinear fields are always in the left hemisphere and for this reason, the collinear particles do not contribute to ω_R. According to its definition the jet function transforms as $J \to J/\alpha$ under the transformation

$$\bar{n} \to \alpha\, \bar{n}\,, \qquad\qquad \omega_L \to \alpha\, \omega_L\,, \tag{A.3}$$

or equivalently

$$J(\alpha\, \omega_L) = \frac{1}{\alpha} J(\omega_L)\,. \tag{A.4}$$

The n-loop corrections to $J(\alpha\, \omega_L)$ scale as $\omega_L^{-1-2n\epsilon}$ and are thus incompatible with this scaling relation (A.4). We conclude that they must all vanish so that $J(\omega_L) = \delta(\omega_L)$ to all orders. The leading-power jet function is thus trivial and can be omitted. We note that power corrections do involve nontrivial collinear contributions, as can be checked through an explicit computation of the hemisphere soft function using the method of regions.

B Bare ingredients for the hemisphere soft function

In the main text, we have mostly presented renormalized results and have reconstructed the renormalized hemisphere soft function by combining renormalized ingredients. For completeness, we list here also the bare functions. These can be extracted from the results in [9, 10] and they are used in appendix C to derive the renormalized expressions.

The renormalization is interesting from an effective theory point of view and key to perform the resummation. However, to obtain the fixed-order result one can also combine the bare ingredients given in this appendix to recover the bare hemisphere soft function. The bare ingredients are also what is obtained when performing the method of regions computation. At NNLO, the regions computation yields three terms: i) purely hard contributions, ii) purely soft ones, and iii) a mixed contribution with one hard gluon on the right and a soft one on the left. We now list these in turn.

Let us first give the result for the purely hard corrections. They consist of a double-real emission part and a virtual correction to single gluon emission. In the effective theory

JHEP12(2016)018

language they are

$$\langle \widetilde{\boldsymbol{\mathcal{H}}}_1^{S(2)}(\hat{\theta}_1, \tau_R, \epsilon) \otimes \mathbf{1} \rangle = \left(\frac{\mu}{\tau_R}\right)^{4\epsilon} C_F C_A v_A, \tag{B.1}$$

$$\langle \widetilde{\boldsymbol{\mathcal{H}}}_2^{S(2)}(\{\underline{n}\}, \tau_R, \epsilon) \otimes \mathbf{1} \rangle = \left(\frac{\mu}{\tau_R}\right)^{4\epsilon} \left[C_F^2 h_F^2/2 + C_F C_A h_A + C_F T_F n_f h_f\right]. \tag{B.2}$$

When integrating also over the angles to compute these terms, one recovers the standard phase-space integration and the evaluation of these contributions simply amounts to computing the corrections to the Wilson line matrix element (2.4) in which all particles fly into the right hemisphere. This computation was performed in [9, 10] and we can extract the coefficients h_F, h_A, h_f and v_A from those papers. The results are

$$\begin{aligned}
h_F &= -\frac{2}{\epsilon^2} - \frac{\pi^2}{2} - \frac{14\zeta_3}{3}\epsilon - \frac{7\pi^4}{48}\epsilon^2, \\
h_A &= -\frac{1}{\epsilon^4} - \frac{11}{6\epsilon^3} + \frac{1}{\epsilon^2}\left(-\frac{67}{18} - \pi^2\right) + \frac{1}{\epsilon}\left(-\frac{193}{27} - \frac{11\pi^2}{4} - \frac{35\zeta_3}{3}\right) - \frac{1196}{81} - \frac{67\pi^2}{12} \\
&\quad - \frac{473\zeta_3}{9} - \frac{31\pi^4}{40}, \\
h_f &= \frac{2}{3\epsilon^3} + \frac{10}{9\epsilon^2} + \frac{1}{\epsilon}\left(\frac{38}{27} + \pi^2\right) + \frac{238}{81} + \frac{5\pi^2}{3} + \frac{172\,\zeta_3}{9}, \\
v_A &= \frac{1}{\epsilon^4} + \frac{5\,\pi^2}{6\,\epsilon^2} + \frac{56\,\zeta_3}{3\,\epsilon} + \frac{113\,\pi^4}{120}.
\end{aligned} \tag{B.3}$$

While the results above are related to hard gluon emissions into the right hemisphere, soft gluons can radiate into either hemisphere. Therefore, unlike at NLO, the result for the NNLO corrections to $\widetilde{\boldsymbol{\mathcal{S}}}_1$ are not simply related to the hard gluon emissions. In fact, one has

$$\widetilde{\boldsymbol{\mathcal{S}}}_1^{(2)}(\tau_L, \epsilon) = \left(\frac{\mu}{\tau_L}\right)^{4\epsilon} \left[C_F^2 h_F^2/2 + C_F C_A s_A + C_F T_F n_f s_f\right], \tag{B.4}$$

with

$$\begin{aligned}
s_A - h_A - v_A &= \frac{1}{\epsilon}\left(-\frac{2}{3} + \frac{22\pi^2}{9} - 4\zeta_3\right) + \frac{40}{9} - \frac{134\pi^2}{27} + \frac{8\pi^4}{45} + \frac{44\zeta_3}{3}, \\
s_f - h_f &= \frac{1}{\epsilon}\left(\frac{4}{3} - \frac{8\pi^2}{9}\right) - \frac{68}{9} - \frac{16\zeta_3}{3} + \frac{64\pi^2}{27}.
\end{aligned} \tag{B.5}$$

The differences quoted above are due to opposite-side emissions only and they contribute to subleading NGLs. These opposite-side contributions can be obtained from the computations in [9, 10] by sending the right hemisphere energy ω_R to infinity because ω_R is much larger than the momentum components of the soft radiation. We have verified that a direct computation of the corresponding diagrams gives the same result.

The final NNLO contribution is the convolution of NLO terms:

$$\langle \widetilde{\boldsymbol{\mathcal{H}}}_1^{S(1)} \otimes \widetilde{\boldsymbol{\mathcal{S}}}_2^{(1)} \rangle(\tau_L, \tau_R, \epsilon) = \left(\frac{\mu}{\tau_L}\right)^{2\epsilon} \left(\frac{\mu}{\tau_R}\right)^{2\epsilon} \left(C_F^2\, p_F + C_F C_A\, p_A\right), \tag{B.6}$$

JHEP12(2016)018

where

$$p_A = \frac{2\pi^2}{3\epsilon^2} + \frac{4\zeta_3}{\epsilon} + \frac{29\pi^4}{45}\,,$$
$$p_F = \frac{4}{\epsilon^4} + \frac{2\pi^2}{\epsilon^2} + \frac{56\zeta_3}{3\epsilon} + \frac{5\pi^4}{6}\,. \tag{B.7}$$

It is worth noting that the product coefficient p_A induced through the convolution of NLO functions is reproduced by the regions calculation of opposite-side gluon contributions, one with a hard scaling and the other with a soft scaling. This type of contribution is responsible for the leading NGLs, as well as part of the subleading ones.

Evaluating the full NNLO expression according to (3.12) then yields

$$\begin{aligned}\widetilde{s}^{(2)}(\tau_L,\tau_R,\epsilon) = &\left[\left(\frac{\mu}{\tau_L}\right)^{4\epsilon} + \left(\frac{\mu}{\tau_R}\right)^{4\epsilon}\right]\left[C_F^2 h_F^2/2 + C_F C_A(h_A+v_A) + C_F T_F n_f h_f\right]\\ &+\left(\frac{\mu}{\tau_L}\right)^{4\epsilon}\left[C_F C_A(s_A - h_A - v_A) + C_F T_F n_f (s_f - h_f)\right]\\ &+\left(\frac{\mu}{\tau_L}\right)^{2\epsilon}\left(\frac{\mu}{\tau_R}\right)^{2\epsilon}\left[C_F C_A p_A + C_F^2 p_F\right]\end{aligned} \tag{B.8}$$

where the same-side contributions are in the first line, and the opposite-side contributions in the second and third.

To obtain the renormalized function, we need to multiply by the renormalization factor $\tilde{Z}_S$ introduced in (3.2). Given the product structure of the factorization theorem (1.3) in Laplace space, it must have a factorized form

$$\tilde{Z}_S(\tau_L,\tau_R,\epsilon,\mu) = \tilde{z}_s(\tau_L,\epsilon,\mu)\tilde{z}_s(\tau_R,\epsilon,\mu)\,, \tag{B.9}$$

where $\tilde{z}_s$ satisfies the RG equation

$$\frac{d}{d\ln\mu}\tilde{z}_s(\tau,\epsilon,\mu) = \left[2\Gamma_{\text{cusp}}\ln\left(\frac{\tau}{\mu}\right) + \gamma_S\right]\tilde{z}_s(\tau,\epsilon,\mu)\,. \tag{B.10}$$

Solving this equation perturbatively gives

$$\begin{aligned}\ln(\tilde{z}_s(\tau,\epsilon,\mu)) = &\frac{\alpha_s}{4\pi}\left[\frac{\Gamma_0}{2\epsilon^2} - \frac{1}{\epsilon}\left(\Gamma_0 L + \frac{\gamma_0^S}{2}\right)\right]\\ &+\left(\frac{\alpha_s}{4\pi}\right)^2\left[-\frac{3\beta_0\Gamma_0}{8\epsilon^3} + \frac{\Gamma_1}{8\epsilon^2} + \frac{1}{2\epsilon^2}\left(\Gamma_0 L + \frac{\gamma_0^S}{2}\right)\beta_0 - \frac{1}{2\epsilon}\left(\Gamma_1 L + \frac{\gamma_1^S}{2}\right)\right],\end{aligned} \tag{B.11}$$

where $L = \ln(\tau/\mu)$. For convenience we give the necessary anomalous dimension in the above expression. The expansion of the anomalous dimensions in the strong coupling constant reads

$$\Gamma_{\text{cusp}} = \sum_{n=0}^{\infty}\left(\frac{\alpha_s}{4\pi}\right)^{n+1}\Gamma_n\,, \qquad \gamma_S = \sum_{n=0}^{\infty}\left(\frac{\alpha_s}{4\pi}\right)^{n+1}\gamma_n^S\,,$$

with

$$\Gamma_0 = 4C_F, \qquad \Gamma_1 = \left(\frac{268}{9} - \frac{4\pi^2}{3}\right)C_F C_A - \frac{80}{9}C_F T_F n_f, \tag{B.12}$$

JHEP12(2016)018

and

$$\gamma_0^S = 0, \quad \gamma_1^S = \left(-\frac{808}{27} + \frac{11\pi^2}{9} + 28\zeta_3\right) C_F C_A + \left(\frac{224}{27} - \frac{4\pi^2}{9}\right) C_F T_F n_f. \tag{B.13}$$

To perform the NLL resummation in section 5 we also need the anomalous dimensions

$$\gamma_0^J = -3C_F\,, \quad \beta_0 = \frac{11}{3}\,C_A - \frac{4}{3}\,T_F n_f\,, \quad \beta_1 = \frac{34}{3}\,C_A^2 - \frac{20}{3}\,C_A T_F n_f - 4C_F T_F n_f\,. \tag{B.14}$$

C NNLO renormalization for the factorized hemisphere soft function

We have presented the renormalization equations for the component hard and soft functions entering the factorization formula for the hemisphere soft function in (3.5) and (3.6). Using that $\widetilde{\boldsymbol{\mathcal{H}}}_0^{S(1)} = \mathbf{1}$ and writing out these equations explicitly to NNLO and suppressing all functional dependence except for μ and ϵ on the right-hand side, we find the relations

$$\begin{aligned}
\widetilde{\boldsymbol{\mathcal{H}}}_1^{S(1)}(\{\underline{n}\}, \tau_R, \mu) &= \widetilde{\boldsymbol{\mathcal{H}}}_1^{S(1)}(\epsilon) - \widetilde{\boldsymbol{\mathcal{Z}}}_{01}^{(1)}(\epsilon, \mu)\,, \\
\widetilde{\boldsymbol{\mathcal{H}}}_1^{S(2)}(\{\underline{n}\}, \tau_R, \mu) &= \widetilde{\boldsymbol{\mathcal{H}}}_1^{S(2)}(\epsilon) - \widetilde{\boldsymbol{\mathcal{Z}}}_{01}^{(2)}(\epsilon, \mu) + \widetilde{\boldsymbol{\mathcal{Z}}}_{01}^{(1)}(\epsilon, \mu)\widetilde{\boldsymbol{\mathcal{Z}}}_{11}^{(1)}(\epsilon, \mu) \\
&\quad - \widetilde{\boldsymbol{\mathcal{H}}}_1^{S(1)}(\epsilon)\left[\widetilde{\boldsymbol{\mathcal{Z}}}_{11}^{(1)}(\epsilon, \mu) + \frac{\beta_0}{\epsilon}\right], \\
\widetilde{\boldsymbol{\mathcal{H}}}_2^{S(2)}(\{\underline{n}\}, \tau_R, \mu) &= \widetilde{\boldsymbol{\mathcal{H}}}_2^{S(2)}(\epsilon) - \widetilde{\boldsymbol{\mathcal{Z}}}_{02}^{(2)}(\epsilon, \mu) + \widetilde{\boldsymbol{\mathcal{Z}}}_{01}^{(1)}(\epsilon, \mu)\widetilde{\boldsymbol{\mathcal{Z}}}_{12}^{(1)}(\epsilon, \mu) - \widetilde{\boldsymbol{\mathcal{H}}}_1^{S(1)}(\epsilon)\widetilde{\boldsymbol{\mathcal{Z}}}_{12}^{(1)}(\epsilon, \mu)\,,
\end{aligned} \tag{C.1}$$

where the term involving β_0 arises because the bare functions were expanded in the bare coupling instead of the renormalized one. Similarly, for the soft function we find

$$\begin{aligned}
\widetilde{\boldsymbol{\mathcal{S}}}_1^{(1)}(\{\underline{n}\}, \tau_L, \mu) &= \left[\tilde{Z}_S(\epsilon, \mu)\widetilde{\boldsymbol{\mathcal{S}}}_1(\epsilon)\right]^{(1)} + \widetilde{\boldsymbol{\mathcal{Z}}}_{01}^{(1)}(\epsilon, \mu)\hat{\otimes}\mathbf{1}\,, \\
\widetilde{\boldsymbol{\mathcal{S}}}_1^{(2)}(\{\underline{n}\}, \tau_L, \mu) &= \left[\tilde{Z}_S(\epsilon, \mu)\widetilde{\boldsymbol{\mathcal{S}}}_1(\epsilon)\right]^{(2)} + \widetilde{\boldsymbol{\mathcal{Z}}}_{01}^{(1)}\hat{\otimes}\left[\tilde{Z}_S(\epsilon, \mu)\widetilde{\boldsymbol{\mathcal{S}}}_2(\epsilon)\right]^{(1)} \\
&\quad + \left(\widetilde{\boldsymbol{\mathcal{Z}}}_{01}^{(2)}(\epsilon, \mu) + \widetilde{\boldsymbol{\mathcal{Z}}}_{02}^{(2)}(\epsilon, \mu)\right)\hat{\otimes}\mathbf{1}\,, \\
\widetilde{\boldsymbol{\mathcal{S}}}_2^{(1)}(\{\underline{n}\}, \tau_L, \mu) &= \left[\tilde{Z}_S(\epsilon, \mu)\widetilde{\boldsymbol{\mathcal{S}}}_2(\epsilon)\right]^{(1)} + \widetilde{\boldsymbol{\mathcal{Z}}}_{11}^{(1)}(\epsilon, \mu) + \widetilde{\boldsymbol{\mathcal{Z}}}_{12}^{(1)}(\epsilon, \mu)\hat{\otimes}\mathbf{1}\,.
\end{aligned} \tag{C.2}$$

Here $[\ldots]^{(2)}$ and $\widetilde{\boldsymbol{\mathcal{Z}}}_{lm}^{(2)}$ refer to the second-order coefficients in the renormalized coupling, while $\widetilde{\boldsymbol{\mathcal{S}}}_1^{(2)}(\epsilon)$ denotes the second order coefficient of the bare coupling. Notice that $\widetilde{\boldsymbol{\mathcal{S}}}_2^{(1)}$ is a regular function in its arguments, so the equations above imply that $\widetilde{\boldsymbol{\mathcal{Z}}}_{12}^{(1)}$ and $\widetilde{\boldsymbol{\mathcal{Z}}}_{11}^{(1)}$ are also regular functions and not distributions. It follows that the renormalized NLO functions are simply obtained from the bare functions by dropping the poles. Moreover, the following

JHEP12(2016)018

linear combinations of renormalization factors are immediately obtained

$$\langle \widetilde{\boldsymbol{\mathcal{Z}}}_{11}^{(1)}(\epsilon,\mu) + \widetilde{\boldsymbol{\mathcal{Z}}}_{12}^{(1)}(\epsilon,\mu)\hat{\otimes}\mathbf{1}\rangle = C_F\left[-\frac{2}{\epsilon^2}+\frac{4}{\epsilon}L_R\right] - 2\,C_A\frac{\ln(1-\hat{\theta}_1^2)}{\epsilon}\,,$$

$$\begin{aligned}\big\langle\big[\widetilde{\boldsymbol{\mathcal{Z}}}_{01}^{(2)}(\epsilon,\mu) + \widetilde{\boldsymbol{\mathcal{Z}}}_{02}^{(2)}(\epsilon,\mu)\big]\hat{\otimes}\mathbf{1}\big\rangle &= C_F^2\left[\frac{2}{\epsilon^4}-\frac{8}{\epsilon^3}L_R+\frac{8}{\epsilon^2}L_R^2\right]\\ &+ C_A C_F\left[\frac{11}{2\epsilon^3}-\frac{1}{\epsilon^2}\left(\frac{67}{18}+\frac{\pi^2}{6}+\frac{22}{3}L_R\right)+\frac{1}{\epsilon}\left(-\frac{193}{27}-\frac{11\pi^2}{12}+3\zeta_3+\left(\frac{134}{9}-\frac{2\pi^2}{3}\right)L_R\right)\right]\\ &+ C_F T_F n_f\left[-\frac{2}{\epsilon^3}+\frac{1}{\epsilon^2}\left(\frac{10}{9}+\frac{8}{3}L_R\right)+\frac{1}{\epsilon}\left(\frac{38}{27}+\frac{\pi^2}{3}-\frac{40}{9}L_R\right)\right].\end{aligned} \tag{C.3}$$

For the renormalized soft function we obtain the result in (3.22). Because only the linear combinations of renormalization factors listed in (C.3) above is determined, and because we have the bare functions only after integrating over angles, we can only determine the combination $\langle \widetilde{\boldsymbol{\mathcal{H}}}_1^{S(2)}(\{\underline{n}\},\tau_R,\mu)\otimes\mathbf{1} + \widetilde{\boldsymbol{\mathcal{H}}}_2^{S(2)}(\{\underline{n}\},\tau_R,\mu)\otimes\mathbf{1}\rangle$ of NNLO hard functions. The result for this combination was given in (3.31).

D Bare ingredients for the light-jet mass

In the main text, we provided the ingredients to obtain the light-jet mass distribution from renormalized quantities, but equally well one can construct the result starting from their bare counterparts. To this end, we collect here all the two-loop bare ingredients for the light-jet mass case. The bare hard function $H(Q,\epsilon)$ and soft function $\widetilde{\boldsymbol{\mathcal{S}}}_1(\tau,\epsilon)$ have been given in appendix A of [20] and we only list the new two-loop ingredients. The first is one-loop bare hard function $\boldsymbol{\mathcal{H}}_2^{(1)}$ convoluted with the trivial leading-order soft function

$$\begin{aligned}\sum_{i=q,\bar{q}}\langle\boldsymbol{\mathcal{H}}_2^{i,(1)}\otimes\mathbf{1}\rangle &= C_F\sigma_0\left(\frac{\mu}{Q}\right)^{2\epsilon}\left[\frac{2}{\epsilon^2}+\frac{3}{\epsilon}+\frac{29}{3}-\frac{3\pi^2}{2}-2\ln^2 2+\frac{5\ln 3}{4}-4\,\mathrm{Li}_2\left(-\frac{1}{2}\right)\right.\\ &+\epsilon\left(\frac{169}{6}-\frac{11\pi^2}{6}-\frac{76\zeta_3}{3}+\frac{32\ln^3 2}{3}-\frac{7\ln^2 2}{4}-18\ln^2 2\ln 3+\frac{15\ln^2 3}{8}\right.\\ &+6\ln 2\ln^2 3-\frac{4}{3}\pi^2\ln 2+\frac{39\ln 3}{8}-\frac{7}{2}\,\mathrm{Li}_2\left(-\frac{1}{2}\right)-12\mathrm{Li}_2\left(-\frac{1}{2}\right)\ln 3\\ &\left.\left.-16\,\mathrm{Li}_3\left(-\frac{1}{2}\right)-6\,\mathrm{Li}_3\left(\frac{3}{4}\right)\right)+\mathcal{O}(\epsilon^2)\right],\\ \langle\boldsymbol{\mathcal{H}}_2^{g,(1)}\otimes\mathbf{1}\rangle &= C_F\sigma_0\left(\frac{\mu}{Q}\right)^{2\epsilon}\left[-\frac{1}{6}+\frac{\pi^2}{3}+2\ln^2 2-\frac{5\ln 3}{4}+4\,\mathrm{Li}_2\left(-\frac{1}{2}\right)+\epsilon\left(-\frac{11}{12}+\frac{\pi^2}{12}\right.\right.\\ &+\frac{22\zeta_3}{3}-\frac{8\ln^3 2}{3}+\frac{4\ln^3 3}{3}+\frac{7\ln^2 2}{4}+10\ln^2 2\ln 3-\frac{15\ln^2 3}{8}\\ &-6\ln 2\ln^2 3+\frac{4}{3}\pi^2\ln 2-\frac{39\ln 3}{8}+\frac{7}{2}\,\mathrm{Li}_2\left(-\frac{1}{2}\right)+12\,\mathrm{Li}_2\left(-\frac{1}{2}\right)\ln 3\\ &\left.\left.-8\,\mathrm{Li}_3\left(\frac{1}{3}\right)+2\,\mathrm{Li}_3\left(\frac{3}{4}\right)\right)+\mathcal{O}(\epsilon^2)\right].\end{aligned} \tag{D.1}$$

JHEP12(2016)018

Each of the results includes transcendental numbers other than ζ-values, but they exactly cancel out in the sum of both contributions. For completeness we also list the bare jet functions in Laplace space. The two-loop quark jet function reads

$$\tilde{j}_{q,\text{bare}}(\tau Q,\epsilon)=1+\frac{\alpha_0 C_F}{4\pi}\left(\frac{\mu^2}{\tau Q}\right)^{\epsilon}\left[\frac{4}{\epsilon^2}+\frac{3}{\epsilon}+7-\frac{2\pi^2}{3}+\epsilon\left(14-\frac{\pi^2}{2}-8\zeta_3\right)\right. \tag{D.2}$$
$$\left.+\epsilon^2\left(28-\frac{7\pi^2}{6}-6\zeta_3-\frac{\pi^4}{10}\right)\right]+\left(\frac{\alpha_0}{4\pi}\right)^2\left(\frac{\mu^2}{\tau Q}\right)^{2\epsilon}\left(C_F^2 j_F+C_F C_A j_A+C_F T_F n_f j_f\right),$$

with

$$\begin{aligned}
j_F &= \frac{8}{\epsilon^4}+\frac{12}{\epsilon^3}+\frac{1}{\epsilon^2}\left(\frac{65}{2}-\frac{8\pi^2}{3}\right)+\frac{1}{\epsilon}\left(\frac{311}{4}-5\pi^2-20\zeta_3\right)+\frac{1437}{8}-\frac{57\pi^2}{4}-54\zeta_3+\frac{5\pi^4}{18},\\
j_A &= \frac{11}{3\epsilon^3}+\frac{1}{\epsilon^2}\left(\frac{233}{18}-\frac{\pi^2}{3}\right)+\frac{1}{\epsilon}\left(\frac{4541}{108}-\frac{11\pi^2}{6}-20\zeta_3\right)+\frac{86393}{648}-\frac{221\pi^2}{36}-\frac{142\zeta_3}{3}-\frac{37\pi^4}{180},\\
j_f &= -\frac{4}{3\epsilon^3}-\frac{38}{9\epsilon^2}+\frac{1}{\epsilon}\left(-\frac{373}{27}+\frac{2\pi^2}{3}\right)-\frac{7081}{162}+\frac{19\pi^2}{9}+\frac{32\zeta_3}{3},
\end{aligned} \tag{D.3}$$

and the one-loop gluon result has the form

$$\tilde{j}_{g,\text{bare}}(\tau Q,\epsilon)=1+\frac{\alpha_0}{4\pi}\left(\frac{\mu^2}{\tau Q}\right)^{\epsilon}\left[C_A\left(\frac{4}{\epsilon^2}+\frac{11}{3\epsilon}+\frac{67}{9}-\frac{2\pi^2}{3}\right)+T_F n_f\left(-\frac{4}{3\epsilon}-\frac{20}{9}\right)\right]. \tag{D.4}$$

Next, we consider the convolution of the one-loop hard and soft functions. Since we are only interested in the logarithmic terms in the cross section, it is sufficient to give the divergent parts of the convolution, which have the form

$$\begin{aligned}
\sum_{i=q,\bar{q}}\left\langle \boldsymbol{\mathcal{H}}_2^{i(1)}\otimes\widetilde{\boldsymbol{\mathcal{S}}}_2^{(1)}\right\rangle_{\text{div.}} &= \left(\frac{\mu^2}{\tau Q}\right)^{2\epsilon}\sigma_0\left[C_F^2\left(-\frac{4}{\epsilon^4}-\frac{6}{\epsilon^3}+\frac{M_{F,q}^{[-2]}}{\epsilon^2}+\frac{M_{F,q}^{[-1]}}{\epsilon}\right)\right.\\
&\qquad\left.+C_F C_A\left(\frac{2\pi^2}{3\epsilon^2}+\frac{M_{A,q}^{[-1]}}{\epsilon}\right)\right],\\
\left\langle \boldsymbol{\mathcal{H}}_2^{g(1)}\otimes\widetilde{\boldsymbol{\mathcal{S}}}_2^{(1)}\right\rangle_{\text{div.}} &= \left(\frac{\mu^2}{\tau Q}\right)^{2\epsilon}\sigma_0\left[C_F^2\left(\frac{M_{F,g}^{[-1]}}{\epsilon}\right)+C_F C_A\left(\frac{M_{A,g}^{[-2]}}{\epsilon^2}+\frac{M_{A,g}^{[-1]}}{\epsilon}\right)\right],
\end{aligned} \tag{D.5}$$

JHEP12(2016)018

with

$$
\begin{aligned}
M^{[-2]}_{F,\,q} &= -\frac{58}{3} + 2\pi^2 + 4\ln^2 2 - \frac{5}{2}\ln 3 + 8\,\mathrm{Li}_2\left(-\frac{1}{2}\right),\\
M^{[-1]}_{F,\,q} &= -\frac{395}{6} + \frac{23\pi^2}{4} + \frac{167\zeta_3}{6} - \frac{92\ln^3 2}{3} + \frac{41\ln^2 2}{4} + 48\ln^2 2\ln 3 - 5\ln^2 3 - 16\ln 2\ln^2 3\\
&\quad + \frac{28\ln 2}{3} + 4\pi^2\ln 2 - \frac{337\ln 3}{12} + \frac{5}{2}\ln 2\ln 3 + \frac{73}{2}\,\mathrm{Li}_2\left(-\frac{1}{2}\right) - 8\,\mathrm{Li}_2\left(-\frac{1}{2}\right)\ln 2\\
&\quad + 32\,\mathrm{Li}_2\left(-\frac{1}{2}\right)\ln 3 + 32\,\mathrm{Li}_3\left(-\frac{1}{2}\right) + 16\,\mathrm{Li}_3\left(\frac{3}{4}\right),\\
M^{[-1]}_{A,\,q} &= \frac{33}{8} - \frac{7\pi^2}{2} + 76\zeta_3 + \frac{64\ln^3 2}{3} + 8\ln 2\ln^2 3 + \frac{5\ln^2 3}{2} - 24\ln^2 2\ln 3 - \frac{33\ln^2 2}{2}\\
&\quad + \frac{39}{2}\ln 2\ln 3 + \frac{359\ln 3}{12} - \frac{8}{3}\pi^2\ln 2 - 52\ln 2 - 65\,\mathrm{Li}_2\left(-\frac{1}{2}\right) - 16\,\mathrm{Li}_2\left(-\frac{1}{2}\right)\ln 3\\
&\quad + 40\,\mathrm{Li}_2\left(-\frac{1}{2}\right)\ln 2 - 8\,\mathrm{Li}_3\left(\frac{3}{4}\right) + 56\,\mathrm{Li}_3\left(-\frac{1}{2}\right) + 8\,I_1\,,
\end{aligned}
\tag{D.6}
$$

and

$$
\begin{aligned}
M^{[-1]}_{F,\,g} &= -2 - \frac{55\,\pi^2}{12} - \frac{364\,\zeta_3}{3} - 20\ln^3 2 - 4\ln 2\ln^2 3 - \frac{5\ln^2 3}{4} + 12\ln^2 2\ln 3 - \frac{69\ln^2 2}{4}\\
&\quad + \frac{51}{2}\ln 2\ln 3 - \frac{23\ln 3}{6} + \frac{16}{3}\pi^2\ln 2 + 20\ln 2 - \frac{133}{2}\,\mathrm{Li}_2\left(-\frac{1}{2}\right) + 8\,\mathrm{Li}_2\left(-\frac{1}{2}\right)\ln 3\\
&\quad - 88\,\mathrm{Li}_2\left(-\frac{1}{2}\right)\ln 2 + 4\,\mathrm{Li}_3\left(\frac{3}{4}\right) - 176\,\mathrm{Li}_3\left(-\frac{1}{2}\right) + 8\,I_2\,,\\
M^{[-2]}_{A,\,g} &= \frac{1}{3} - \frac{2\pi^2}{3} - 4\ln^2 2 + \frac{5\ln 3}{2} - 8\,\mathrm{Li}_2\left(-\frac{1}{2}\right),\\
M^{[-1]}_{A,\,g} &= \frac{13}{3} + \pi^2 + 47\zeta_3 + 36\ln^3 2 + \frac{23\ln^2 2}{4} - 48\ln^2 2\ln 3 + 5\ln^2 3 + 16\ln 2\ln^2 3 - \frac{56\ln 2}{3}\\
&\quad - 6\pi^2\ln 2 + \frac{61\ln 3}{3} - 14\ln 2\ln 3 + \frac{23}{2}\,\mathrm{Li}_2\left(-\frac{1}{2}\right) + 56\,\mathrm{Li}_3\left(-\frac{1}{2}\right) - 16\,\mathrm{Li}_3\left(\frac{3}{4}\right)\\
&\quad + 48\,\mathrm{Li}_2\left(-\frac{1}{2}\right)\ln 2 - 32\mathrm{Li}_2\left(-\frac{1}{2}\right)\ln 3\,.
\end{aligned}
\tag{D.7}
$$

The result for the coefficients involves two angular integrals I_1 and I_2 which we were not able to evaluate in closed form. They are

$$
\begin{aligned}
I_1 &= \int_0^{1/\sqrt{3}} d\hat{\theta}_2 \int_{\hat{\theta}_2}^{-\hat{\theta}_2+\sqrt{1+\hat{\theta}_2^2}} d\hat{\theta}_1\, f(\hat{\theta}_1,\hat{\theta}_2)\ln(1-\hat{\theta}_2^2) = -0.0423782819\,,\\
I_2 &= \int_0^{1/\sqrt{3}} d\hat{\theta}_2 \int_{\hat{\theta}_2}^{-\hat{\theta}_2+\sqrt{1+\hat{\theta}_2^2}} d\hat{\theta}_1\, g(\hat{\theta}_1,\hat{\theta}_2)\ln(1-\hat{\theta}_2^2) = -0.0145491799\,,
\end{aligned}
\tag{D.8}
$$

with

$$
\begin{aligned}
f(\hat{\theta}_1,\hat{\theta}_2) &= \frac{2\hat{\theta}_1\hat{\theta}_2(1-\hat{\theta}_1^2)(1-\hat{\theta}_2^2) + 2\hat{\theta}_2^2(1+\hat{\theta}_1^4) + \hat{\theta}_1^2(1-\hat{\theta}_2^2)^2}{\hat{\theta}_1(\hat{\theta}_1+\hat{\theta}_2)^3}\,,\\
g(\hat{\theta}_1,\hat{\theta}_2) &= \frac{\hat{\theta}_1^2(1+\hat{\theta}_2^2)^2 + \hat{\theta}_2^2(1+\hat{\theta}_1^2)^2}{(\hat{\theta}_1+\hat{\theta}_2)^2(1-\hat{\theta}_1\hat{\theta}_2)}\,.
\end{aligned}
\tag{D.9}
$$

JHEP12(2016)018

In the main text, we considered in the convolution of the renormalized one-loop hard and soft functions. The form of the convolution was given in (4.10) and (4.11). The coefficients of the logarithmic terms in these two formulas are closely related the coefficients of the divergences given above. Explicitly, they read

$$
\begin{aligned}
M_{q,F}^{(2)} &= -\frac{116}{3} + 6\,\pi^2 + 8\ln^2 2 - 5\ln 3 + 16\,\mathrm{Li}_2\left(-\frac{1}{2}\right), \\
M_{q,F}^{(1)} &= 19 - \frac{43\,\pi^2}{6} + 27\zeta_3 + \frac{56\ln^3 2}{3} - \frac{27\ln^2 2}{2} - 24\ln^2 2\ln 3 + \frac{5\ln^2 3}{2} + 8\ln 2\ln^2 3 \\
&\quad - \frac{56\ln 2}{3} - \frac{8}{3}\pi^2\ln 2 + \frac{110\ln 3}{3} - 5\ln 2\ln 3 - 59\,\mathrm{Li}_2\left(-\frac{1}{2}\right) - 8\,\mathrm{Li}_3\left(\frac{3}{4}\right) \\
&\quad + 16\,\mathrm{Li}_2\left(-\frac{1}{2}\right)\ln 2 - 16\,\mathrm{Li}_2\left(-\frac{1}{2}\right)\ln 3\,, \\
M_{q,A}^{(1)} &= -\frac{33}{4} + 7\pi^2 - 136\zeta_3 - \frac{128\ln^3 2}{3} - 16\ln 2\ln^2 3 - 5\ln^2 3 + 48\ln^2 2\ln 3 + 33\ln^2 2 \\
&\quad - 39\ln 2\ln 3 - \frac{359\ln 3}{6} + \frac{16}{3}\pi^2\ln 2 + 104\ln 2 + 130\,\mathrm{Li}_2\left(-\frac{1}{2}\right) + 32\,\mathrm{Li}_2\left(-\frac{1}{2}\right)\ln 3 \\
&\quad - 80\,\mathrm{Li}_2\left(-\frac{1}{2}\right)\ln 2 + 16\,\mathrm{Li}_3\left(\frac{3}{4}\right) - 112\,\mathrm{Li}_3\left(-\frac{1}{2}\right) - 16\,I_1\,, \\
M_{g,F}^{(1)} &= 4 + \frac{55\pi^2}{6} + \frac{728\zeta_3}{3} + 40\ln^3 2 + 8\ln 2\ln^2 3 + \frac{5\ln^2 3}{2} - 24\ln^2 2\ln 3 + \frac{69\ln^2 2}{2} \\
&\quad - 51\ln 2\ln 3 + \frac{23\ln 3}{3} - \frac{32}{3}\pi^2\ln 2 - 40\ln 2 + 133\,\mathrm{Li}_2\left(-\frac{1}{2}\right) - 16\,\mathrm{Li}_2\left(-\frac{1}{2}\right)\ln 3 \\
&\quad + 176\,\mathrm{Li}_2\left(-\frac{1}{2}\right)\ln 2 - 8\,\mathrm{Li}_3\left(\frac{3}{4}\right) + 352\,\mathrm{Li}_3\left(-\frac{1}{2}\right) - 16\,I_2\,, \\
M_{g,A}^{(2)} &= \frac{2}{3} - \frac{4\pi^2}{3} - 8\ln^2 2 + 5\ln 3 - 16\,\mathrm{Li}_2\left(-\frac{1}{2}\right), \\
M_{g,A}^{(1)} &= -5 - \frac{7\pi^2}{3} - \frac{386\,\zeta_3}{3} - \frac{88\ln^3 2}{3} - \frac{37\ln^2 2}{2} + 24\ln^2 2\ln 3 - \frac{5\ln^2 3}{2} - 8\ln 2\ln^2 3 \\
&\quad + \frac{112\ln 2}{3} + \frac{20}{3}\pi^2\ln 2 - \frac{127\ln 3}{6} + 28\ln 2\ln 3 - 37\,\mathrm{Li}_2\left(-\frac{1}{2}\right) - 176\,\mathrm{Li}_3\left(-\frac{1}{2}\right) \\
&\quad + 8\,\mathrm{Li}_3\left(\frac{3}{4}\right) - 96\,\mathrm{Li}_2\left(-\frac{1}{2}\right)\ln 2 + 16\,\mathrm{Li}_2\left(-\frac{1}{2}\right)\ln 3\,. \qquad \text{(D.10)}
\end{aligned}
$$

Since we are only interested in the logarithmic terms in the cross section, we do not list the results for the constants $M_X^{(0)}$.

Finally, the divergent part of two-loop hard functions $\boldsymbol{\mathcal{H}}_2^{(2)}$ and $\boldsymbol{\mathcal{H}}_3^{(2)}$ can be inferred from the requirement that the cross section is finite. The finiteness condition implies that the divergences are given by

$$
\begin{aligned}
\sum_{i=q,\bar{q}} \langle \boldsymbol{\mathcal{H}}_2^{i,(2)} \otimes \mathbf{1} + \boldsymbol{\mathcal{H}}_3^{i,(2)} \otimes \mathbf{1} \rangle_{\text{div.}} &= \left(\frac{\mu}{Q}\right)^{4\epsilon} \sigma_0 \left(C_F^2 H_{F,q} + C_F C_A H_{A,q} + C_F T_F n_f H_{f,q}\right), \\
\langle \boldsymbol{\mathcal{H}}_2^{g,(2)} \otimes \mathbf{1} + \boldsymbol{\mathcal{H}}_3^{g,(2)} \otimes \mathbf{1} \rangle_{\text{div.}} &= \left(\frac{\mu}{Q}\right)^{4\epsilon} \sigma_0 \left(C_F^2 H_{F,g} + C_F C_A H_{A,g}\right). \qquad \text{(D.11)}
\end{aligned}
$$

JHEP12(2016)018

The second-order coefficients of the different color structures for the quark and gluon contributions read

$$
\begin{aligned}
H_{F,q} = &-\frac{6}{\epsilon^4} - \frac{18}{\epsilon^3} + \frac{1}{\epsilon^2}\left[-\frac{389}{6} + \frac{23\pi^2}{3} + 4\ln^2 2 - \frac{5\ln 3}{2} + 8\,\mathrm{Li}_2\left(-\frac{1}{2}\right)\right] + \frac{1}{\epsilon}\Bigg[-\frac{2245}{12} \\
&+ \frac{211\pi^2}{12} + \frac{569\zeta_3}{6} - 12\ln^3 2 + \frac{11\ln^2 2}{4} + 24\ln^2 2\ln 3 - \frac{5\ln^2 3}{2} - 8\ln 2\ln^2 3 - \frac{28\ln 2}{3} \\
&+ \frac{4}{3}\pi^2\ln 2 + \frac{29\ln 3}{6} - \frac{5}{2}\ln 2\ln 3 - \frac{21}{2}\,\mathrm{Li}_2\left(-\frac{1}{2}\right) + 8\,\mathrm{Li}_2\left(-\frac{1}{2}\right)\ln 2 \\
&+ 16\,\mathrm{Li}_2\left(-\frac{1}{2}\right)\ln 3 + 32\,\mathrm{Li}_3\left(-\frac{1}{2}\right) + 8\,\mathrm{Li}_3\left(\frac{3}{4}\right)\Bigg], \\
H_{A,q} = &\frac{11}{6\epsilon^3} + \frac{1}{\epsilon^2}\left(\frac{83}{9} - \frac{\pi^2}{2}\right) + \frac{1}{\epsilon}\Bigg[\frac{8759}{216} - \frac{83\pi^2}{36} - 85\zeta_3 - \frac{64\ln^3 2}{3} - 8\ln 2\ln^2 3 - \frac{5\ln^2 3}{2} \\
&+ 24\ln^2 2\ln 3 + \frac{55\ln^2 2}{6} - \frac{39}{2}\ln 2\ln 3 - \frac{76\ln 3}{3} + \frac{8}{3}\pi^2\ln 2 + 52\ln 2 + 8\,\mathrm{Li}_3\left(\frac{3}{4}\right) \\
&- 56\,\mathrm{Li}_3\left(-\frac{1}{2}\right) + \frac{151}{3}\mathrm{Li}_2\left(-\frac{1}{2}\right) + 16\,\mathrm{Li}_2\left(-\frac{1}{2}\right)\ln 3 - 40\,\mathrm{Li}_2\left(-\frac{1}{2}\right)\ln 2 - 8\,I_1\Bigg], \\
H_{f,q} = &-\frac{2}{3\epsilon^3} - \frac{28}{9\epsilon^2} + \frac{1}{\epsilon}\left[-\frac{431}{27} + \frac{19\pi^2}{9} + \frac{8\ln^2 2}{3} - \frac{5\ln 3}{3} + \frac{16}{3}\,\mathrm{Li}_2\left(-\frac{1}{2}\right)\right], \qquad \text{(D.12)} \\
H_{F,g} = &\frac{1}{\epsilon}\Bigg[2 + \frac{55\pi^2}{12} + \frac{364\zeta_3}{3} + 20\ln^3 2 + 4\ln 2\ln^2 3 + \frac{5\ln^2 3}{4} - 12\ln^2 2\ln 3 + \frac{69\ln^2 2}{4} \\
&- \frac{51}{2}\ln 2\ln 3 + \frac{23\ln 3}{6} - \frac{16}{3}\pi^2\ln 2 - 20\ln 2 + \frac{133}{2}\,\mathrm{Li}_2\left(-\frac{1}{2}\right) - 8\,\mathrm{Li}_2\left(-\frac{1}{2}\right)\ln 3 \\
&+ 88\,\mathrm{Li}_2\left(-\frac{1}{2}\right)\ln 2 - 4\,\mathrm{Li}_3\left(\frac{3}{4}\right) + 176\,\mathrm{Li}_3\left(-\frac{1}{2}\right) - 8\,I_2\Bigg], \\
H_{A,g} = &\frac{1}{\epsilon^2}\left[\frac{1}{3} - \frac{2\pi^2}{3} - 4\ln^2 2 + \frac{5\ln 3}{2} - 8\mathrm{Li}_2\left(-\frac{1}{2}\right)\right] + \frac{1}{\epsilon}\Bigg[-\frac{2}{3} - \frac{4\pi^2}{3} - \frac{229\zeta_3}{3} - \frac{76\ln^3 2}{3} \\
&- \frac{16\ln^3 3}{3} - \frac{51\ln^2 2}{4} + 8\ln^2 2\ln 3 + \frac{5\ln^2 3}{2} + 8\ln 2\ln^2 3 + \frac{56\ln 2}{3} + \frac{2}{3}\pi^2\ln 2 - \frac{5\ln 3}{6} \\
&+ 14\ln 2\ln 3 - \frac{51}{2}\mathrm{Li}_2\left(-\frac{1}{2}\right) - 56\mathrm{Li}_3\left(-\frac{1}{2}\right) - 48\mathrm{Li}_2\left(-\frac{1}{2}\right)\ln 2 - 16\mathrm{Li}_2\left(-\frac{1}{2}\right)\ln 3 \\
&+ 32\,\mathrm{Li}_3\left(\frac{1}{3}\right) + 8\,\mathrm{Li}_3\left(\frac{3}{4}\right)\Bigg]. \qquad \text{(D.13)}
\end{aligned}
$$

JHEP12(2016)018

References

[1] V.V. Sudakov, *Vertex parts at very high-energies in quantum electrodynamics*, *Sov. Phys. JETP* **3** (1956) 65 [INSPIRE].

[2] M. Dasgupta and G.P. Salam, *Accounting for coherence in interjet E_t flow: A case study*, *JHEP* **03** (2002) 017 [hep-ph/0203009] [INSPIRE].

[3] A. Banfi, G. Marchesini and G. Smye, *Away from jet energy flow*, *JHEP* **08** (2002) 006 [hep-ph/0206076] [INSPIRE].

[4] M. Dasgupta and G.P. Salam, *Resummation of nonglobal QCD observables*, *Phys. Lett.* **B 512** (2001) 323 [hep-ph/0104277] [INSPIRE].

[5] C.W. Bauer, S. Fleming, D. Pirjol and I.W. Stewart, *An effective field theory for collinear and soft gluons: Heavy to light decays*, *Phys. Rev.* **D 63** (2001) 114020 [hep-ph/0011336] [INSPIRE].

[6] C.W. Bauer, D. Pirjol and I.W. Stewart, *Soft collinear factorization in effective field theory*, *Phys. Rev.* **D 65** (2002) 054022 [hep-ph/0109045] [INSPIRE].

[7] M. Beneke, A.P. Chapovsky, M. Diehl and T. Feldmann, *Soft collinear effective theory and heavy to light currents beyond leading power*, *Nucl. Phys.* **B 643** (2002) 431 [hep-ph/0206152] [INSPIRE].

[8] T. Becher, A. Broggio and A. Ferroglia, *Introduction to Soft-Collinear Effective Theory*, *Lect. Notes Phys.* **896** (2015) 1 [arXiv:1410.1892] [INSPIRE].

[9] R. Kelley, M.D. Schwartz, R.M. Schabinger and H.X. Zhu, *The two-loop hemisphere soft function*, *Phys. Rev.* **D 84** (2011) 045022 [arXiv:1105.3676] [INSPIRE].

[10] A. Hornig, C. Lee, I.W. Stewart, J.R. Walsh and S. Zuberi, *Non-global Structure of the $O(\alpha_s^2)$ Dijet Soft Function*, *JHEP* **08** (2011) 054 [arXiv:1105.4628] [INSPIRE].

[11] R. Kelley, M.D. Schwartz, R.M. Schabinger and H.X. Zhu, *Jet Mass with a Jet Veto at Two Loops and the Universality of Non-Global Structure*, *Phys. Rev.* **D 86** (2012) 054017 [arXiv:1112.3343] [INSPIRE].

[12] A. von Manteuffel, R.M. Schabinger and H.X. Zhu, *The Complete Two-Loop Integrated Jet Thrust Distribution In Soft-Collinear Effective Theory*, *JHEP* **03** (2014) 139 [arXiv:1309.3560] [INSPIRE].

[13] M.D. Schwartz and H.X. Zhu, *Nonglobal logarithms at three loops, four loops, five loops and beyond*, *Phys. Rev.* **D 90** (2014) 065004 [arXiv:1403.4949] [INSPIRE].

[14] K. Khelifa-Kerfa and Y. Delenda, *Non-global logarithms at finite N_c beyond leading order*, *JHEP* **03** (2015) 094 [arXiv:1501.00475] [INSPIRE].

[15] S. Caron-Huot and M. Herranen, *High-energy evolution to three loops*, arXiv:1604.07417 [INSPIRE].

[16] S. Caron-Huot, unpublished.

[17] A.J. Larkoski, I. Moult and D. Neill, *Non-Global Logarithms, Factorization and the Soft Substructure of Jets*, *JHEP* **09** (2015) 143 [arXiv:1501.04596] [INSPIRE].

[18] D. Neill, *The Edge of Jets and Subleading Non-Global Logs*, arXiv:1508.07568 [INSPIRE].

JHEP12(2016)018

[19] A.J. Larkoski, I. Moult and D. Neill, *The Analytic Structure of Non-Global Logarithms: Convergence of the Dressed Gluon Expansion*, *JHEP* **11** (2016) 089 [arXiv:1609.04011] [INSPIRE].

[20] T. Becher, M. Neubert, L. Rothen and D.Y. Shao, *Factorization and Resummation for Jet Processes*, *JHEP* **11** (2016) 019 [arXiv:1605.02737] [INSPIRE].

[21] T. Becher, M. Neubert, L. Rothen and D.Y. Shao, *Effective Field Theory for Jet Processes*, *Phys. Rev. Lett.* **116** (2016) 192001 [arXiv:1508.06645] [INSPIRE].

[22] S. Caron-Huot, *Resummation of non-global logarithms and the BFKL equation*, arXiv:1501.03754 [INSPIRE].

[23] Y.-T. Chien and M.D. Schwartz, *Resummation of heavy jet mass and comparison to LEP data*, *JHEP* **08** (2010) 058 [arXiv:1005.1644] [INSPIRE].

[24] S.J. Burby and E.W.N. Glover, *Resumming the light hemisphere mass and narrow jet broadening distributions in e^+e^- annihilation*, *JHEP* **04** (2001) 029 [hep-ph/0101226] [INSPIRE].

[25] S. Fleming, A.H. Hoang, S. Mantry and I.W. Stewart, *Jets from massive unstable particles: Top-mass determination*, *Phys. Rev.* **D 77** (2008) 074010 [hep-ph/0703207] [INSPIRE].

[26] T. Becher, M. Neubert and B.D. Pecjak, *Factorization and Momentum-Space Resummation in Deep-Inelastic Scattering*, *JHEP* **01** (2007) 076 [hep-ph/0607228] [INSPIRE].

[27] T. Becher, M. Neubert and G. Xu, *Dynamical Threshold Enhancement and Resummation in Drell-Yan Production*, *JHEP* **07** (2008) 030 [arXiv:0710.0680] [INSPIRE].

[28] T. Becher and M. Neubert, *Toward a NNLO calculation of the $\bar{B} \to X_s\gamma$ decay rate with a cut on photon energy. II. Two-loop result for the jet function*, *Phys. Lett.* **B 637** (2006) 251 [hep-ph/0603140] [INSPIRE].

[29] T. Becher and G. Bell, *The gluon jet function at two-loop order*, *Phys. Lett.* **B 695** (2011) 252 [arXiv:1008.1936] [INSPIRE].

[30] P.F. Monni, T. Gehrmann and G. Luisoni, *Two-Loop Soft Corrections and Resummation of the Thrust Distribution in the Dijet Region*, *JHEP* **08** (2011) 010 [arXiv:1105.4560] [INSPIRE].

[31] M. Beneke and V.A. Smirnov, *Asymptotic expansion of Feynman integrals near threshold*, *Nucl. Phys.* **B 522** (1998) 321 [hep-ph/9711391] [INSPIRE].

[32] S. Catani and M.H. Seymour, *The Dipole formalism for the calculation of QCD jet cross-sections at next-to-leading order*, *Phys. Lett.* **B 378** (1996) 287 [hep-ph/9602277] [INSPIRE].

[33] S. Catani and M.H. Seymour, *A General algorithm for calculating jet cross-sections in NLO QCD*, *Nucl. Phys.* **B 485** (1997) 291 [*Erratum ibid.* **B 510** (1998) 503] [hep-ph/9605323] [INSPIRE].

[34] A.H. Hoang and S. Kluth, *Hemisphere Soft Function at $O(\alpha_s^2)$ for Dijet Production in e^+e^- Annihilation*, arXiv:0806.3852 [INSPIRE].

[35] T. Becher and M.D. Schwartz, *A precise determination of α_s from LEP thrust data using effective field theory*, *JHEP* **07** (2008) 034 [arXiv:0803.0342] [INSPIRE].

[36] A. Gehrmann-De Ridder, T. Gehrmann, E.W.N. Glover and G. Heinrich, *NNLO corrections to event shapes in e^+e^- annihilation*, *JHEP* **12** (2007) 094 [arXiv:0711.4711] [INSPIRE].

JHEP12(2016)018

[37] S. Weinzierl, *Event shapes and jet rates in electron-positron annihilation at NNLO*, *JHEP* **06** (2009) 041 [arXiv:0904.1077] [INSPIRE].

[38] V. Del Duca et al., *Jet production in the CoLoRFulNNLO method: event shapes in electron-positron collisions*, *Phys. Rev.* **D 94** (2016) 074019 [arXiv:1606.03453] [INSPIRE].

[39] A. Gehrmann-De Ridder, T. Gehrmann, E.W.N. Glover and G. Heinrich, *EERAD3: Event shapes and jet rates in electron-positron annihilation at order α_s^3*, *Comput. Phys. Commun.* **185** (2014) 3331 [arXiv:1402.4140] [INSPIRE].

[40] T. Becher and X. Garcia i Tormo, *Factorization and resummation for transverse thrust*, *JHEP* **06** (2015) 071 [arXiv:1502.04136] [INSPIRE].

[41] C. Frye, A.J. Larkoski, M.D. Schwartz and K. Yan, *Factorization for groomed jet substructure beyond the next-to-leading logarithm*, *JHEP* **07** (2016) 064 [arXiv:1603.09338] [INSPIRE].

[42] T. Becher and M. Neubert, *Threshold resummation in momentum space from effective field theory*, *Phys. Rev. Lett.* **97** (2006) 082001 [hep-ph/0605050] [INSPIRE].

[43] S. Catani and L. Trentadue, *Resummation of the QCD Perturbative Series for Hard Processes*, *Nucl. Phys.* **B 327** (1989) 323 [INSPIRE].

[44] S. Catani, B.R. Webber and G. Marchesini, *QCD coherent branching and semiinclusive processes at large x*, *Nucl. Phys.* **B 349** (1991) 635 [INSPIRE].

[45] S. Catani, L. Trentadue, G. Turnock and B.R. Webber, *Resummation of large logarithms in e^+e^- event shape distributions*, *Nucl. Phys.* **B 407** (1993) 3 [INSPIRE].

[46] Particle Data Group collaboration, K.A. Olive et al., *Review of Particle Physics*, *Chin. Phys.* **C 38** (2014) 090001 [INSPIRE].

[47] L.G. Almeida, S.D. Ellis, C. Lee, G. Sterman, I. Sung and J.R. Walsh, *Comparing and counting logs in direct and effective methods of QCD resummation*, *JHEP* **04** (2014) 174 [arXiv:1401.4460] [INSPIRE].

[48] ALEPH collaboration, D. Buskulic et al., *Properties of hadronic Z decays and test of QCD generators*, *Z. Phys.* **C 55** (1992) 209 [INSPIRE].

[49] A. Banfi, M. Dasgupta, K. Khelifa-Kerfa and S. Marzani, *Non-global logarithms and jet algorithms in high-p_T jet shapes*, *JHEP* **08** (2010) 064 [arXiv:1004.3483] [INSPIRE].

[50] M. Dasgupta, K. Khelifa-Kerfa, S. Marzani and M. Spannowsky, *On jet mass distributions in Z+jet and dijet processes at the LHC*, *JHEP* **10** (2012) 126 [arXiv:1207.1640] [INSPIRE].

JHEP12(2016)018